

# ‘Spectro-temporal’ characteristics and disk-jet connection of the outbursting black hole source XTE J1859+226

Radhika. D<sup>1,2\*</sup>

<sup>1</sup> *Space Astronomy Group, SSIF, ISRO Satellite Centre, Bengaluru, INDIA*

<sup>2</sup> *Department of Physics, University of Calicut, Kerala, INDIA*

A. Nandi<sup>1</sup>

<sup>1</sup> *Space Astronomy Group, SSIF, ISRO Satellite Centre, Bengaluru, INDIA*

arXiv:1308.3138v3 [astro-ph.HE] 30 Jun 2014

---

## Abstract

We re-investigated the ‘spectro-temporal’ behaviour of the source XTE J1859+226 in X-rays during its outburst phase in 1999, by analysing the RXTE PCA/HEXTE data in 2 - 150 keV spectral band. Detailed analysis shows that the source evolves through different spectral states during its entire outburst as indicated by the variation in the spectral and temporal characteristics. Although the evolution pattern of the outburst followed the typical q-shaped profile, we observed an absence of ‘canonical’ soft state and a weak presence of ‘secondary’ emission during the decay phase of the outburst. The broad-band spectra, modeled with high energy cutoff, shows that the fold-energy increases monotonically in the hard and hard-intermediate states followed by a random variation in the soft-intermediate state. We attempted to estimate the mass of the source based on the evolution of Quasi-Periodic Oscillation (QPO) frequencies during rising phase modeled with the propagating oscillatory shock solution, and from the correlation of photon index and QPO frequency. It is also observed that during multiple ejections (observed as radio flares) the QPO frequencies are not present in the power spectra and there is an absence of lag in the soft to hard photons. The disk flux increases along with a decrease in the high energy flux, implying the soft nature of the spectrum. These results are the ‘possible’ indication that the inner part of the disk (*i.e.*, *Comptonized corona*), which could be responsible for the generation of QPO and for the non-thermal Comptonized component of the spectrum, is disrupted and the matter gets evacuated in the form of jet. We attempted to explain the complex behaviour of ‘spectro-temporal’ properties of the source during the entire outburst and the nature of the disk-jet connection before, during and after the ejection events in the context of two different types of accreting flow material, in presence of magnetic field.

*Keywords:* Black holes, Accretion disks, Radiation hydrodynamics, X-ray Sources, Stars: Individual (XTE J1859+226), Disk-Jet connection

---

## 1. Introduction

Galactic Black Hole (BH) sources are interesting objects to study as these sources are observed only in binaries and the process of accretion gets very complex as the disk evolves with time, especially when the sources undergo outbursts and jet ejections take place. Some of the BH binaries show persistent emission (e.g. Cyg X-1) along with aperiodic X-ray variability (e.g. GRS 1915+105), over more than a period of decade. Some BH sources show outbursting behaviour for shorter duration varying from few days to months, and are called as outbursting BH sources or transients (e.g. GX 339-4, XTE J1118+480, XTE J1748-288, H 1742-322, GRO J1655-40). The

outbursting BH sources show different types of intensity variations (*i.e.*, outburst profile) over different period of time (McClintock & Remilard, 2006). Some of the sources after being quiescent for a long time, show a sudden increase in the intensity level, and attain a maximum intensity within few days and then decay back slowly to quiescence (H 1743-322, A 0620-00, 4U 1543-47). Their light curves have a ‘Fast Rise and Exponential Decay (FRED)’ profile. Some sources have a slow rise to the peak and decay slowly to the quiescence (GX 339-4, XTE J1752-223) and their light curve profile is termed as ‘Slow Rise Slow Decay (SRSD)’. During this whole phenomena, outbursting sources show different spectral and timing variabilities and exhibit different spectral states like *Hard*, *Hard-intermediate*, *Soft-intermediate*, *Soft state* (Homan & Belloni 2005, Belloni 2010) and in some cases a *Very high state* also (Miyamoto et al. 1991, Remilard et al. 1999), in their Hardness-Intensity diagram (HID).

---

\*Corresponding author

Email addresses: radhikad\_isac@yahoo.in (Radhika. D<sup>1,2</sup>), anuj@isac.gov.in (A. Nandi<sup>1</sup>)

It is also observed that in outbursting BH sources, strong jets are emitted which are seen in radio observations (Fender et al., 2004), during the transition from hard-intermediate to soft-intermediate state in the rising phase (e.g. H 1743–322, Miller-Jones et al. 2012) and in the declining phase when the source transits from soft-intermediate to hard state (e.g. XTE J1752–223, Yang et al. 2010). Quasi-simultaneous multiwavelength observations of sources like GX 339–4 (Cadolle Bel et al., 2010), XTE J1748–288 (Brockspop et al., 2007), H 1743–322 (Miller-Jones et al., 2012), strongly suggests that the radio flares emitted are associated with the disk emission. It has been reported from the study of GRS 1915+105 that, during the jet ejections, QPOs are not observed as well as the Comptonized component gets suppressed (Vadawale et al. 2001). This implies that the ‘hot’ Comptonized corona gets disrupted and evacuated, and the source spectra softens, suggesting that the X-ray emission is mostly from the disk (Feroci et al. 1999, Vadawale et al. 2001, Nandi et al. 2001, Chakrabarti et al. 2002, Miller-Jones et al. 2012).

The X-ray transient source XTE J1859+226 was first discovered (Wood et al., 1999) with All Sky Monitor (ASM) onboard Rossi X-ray Timing Explorer (RXTE) (Bradt et al., 1993) on Oct 9, 1999. Subsequently, the source was monitored in X-rays with RXTE/PCA (Proportional Counter Array) and CGRO-BATSE (Compton Gamma Ray Observatory - Burst And Transient Source Experiment) for several months (McCullough & Wilson, 1999). The outburst showed the typical FRED profile. Spectral and temporal characteristics confirmed the source as a black hole candidate (Markwardt, 2001). Several observations in optical and radio wavebands confirmed the presence of the counterpart of the source (Garnavich et al., 1999; Pooley & Hjellming, 1999). Spectroscopic studies of the counterpart showed weak emission lines arising from Balmer series of Hydrogen and He II, which is typical for spectra of LMXBs (Wagner et al., 1999). The mass function was estimated to be  $(4.5 \pm 0.6) M_{\odot}$ , and an assumed inclination angle of  $70^{\circ}$  gave a lower mass limit of  $5.42 M_{\odot}$  (Corral-Santana et al., 2011).

During the 1999 outburst, the source XTE J1859+226 was continuously and extensively monitored in X-rays and in radio, which revealed the X-ray/radio correlations (Brockspop et al., 2002). The source is observed to exhibit multiple flaring events of five in number. From the study of the spectral evolution in radio, it was found that the jet generation is implied by the production of hard X-rays and also that a correlation exists between soft X-ray and radio ejection during the first flare, while a correlation existed between hard X-ray and radio observation during the other ejections. Casella et al. 2004 studied the temporal properties of the source and found that, the QPOs observed can be classified into three types viz. Type A, B and C. This classification scheme based on the QPO characteristics and phase lag, has been considered as one of the basic formalities to classify the QPOs in Black Hole sources (See also Casella et al. 2005; Motta et al. 2011). The phase lag dif-

ference between different types of QPOs, suggests that the shape of oscillation is different in different energies. But the evolution of low frequency QPOs (C-type) as well as their origin during the initial rising phase of the outburst is still not clear.

In the context of disk-jet symbiosis of black hole sources, Fender et al. 2004, 2009 have provided a unified picture along with the estimation of jet power as a function of X-ray luminosity. Their work also highlighted the occurrence of five Radio flares in XTE J1859+226 and suggested that all the flares occur when the source is in a similar spectral state. They found that the rms of the Power density spectra (PDS) reduces during the occurrence of a flare. Rodriguez & Prat 2008 studied the spectral properties of the source during its rising phase and found that the non-thermal flux (2 - 50 keV) remains constant during the first flare of the source. Markwardt 2001 studied the evolution of the source during the rising phase of the outburst and found that there is a signature of partial absence of the QPO (or Comptonized corona), when the first radio flare occurred.

Dunn et al. 2011a,b studied the spectral behaviour of this source in the context of global study of disk dominated states of several BH sources. Considering a simple phenomenological model (diskbb+powerlaw) for BH spectral study, Dunn et al. 2011a showed that a large fraction of disk dominated observations of XTE J1859+226 fall below the ‘standard’ Luminosity-Temperature (L-T) relation (see Gierlinski & Done 2004). Farinelli et al. 2013 has studied the spectral characteristics of the source based on BeppoSAX and RXTE observations, in the context of a bulk motion comptonization model (BMC of XSPEC), and have observed an evolving high energy cut-off component during the hard to soft transition. They have also performed a correlated study between the fraction of Comptonization and the rms variability. But the ‘complex’ evolution of fold energy since the beginning of the outburst along with the evolution of temporal features (QPOs, rms etc.), especially during a radio flare are not explained in detail.

So, in order to have a coherent study of the evolution of temporal and spectral properties of the source (during the entire outburst) as well as the implications on disk dynamics during the multiple ejections, we re-analysed the RXTE PCA/HEXTE temporal and spectral data of the source XTE J1859+226 in the energy band of 2 - 150 keV.

Several models have been proposed to understand the ‘spectro-temporal’ evolution of an outbursting black hole binary. The accretion-ejection instability model (Tagger & Pellat, 1999) and global disk oscillation model (Titarchuk & Osherovich, 2000) attempts to explain the origin of QPOs. Recently, Ingram & Done 2011 based on propagating mass accretion rate fluctuations in hotter inner disk, and Stiele et al. 2013 based on oscillations from a transition layer in between the disk and hot Comptonized flow have proposed alternative models to explain the origin of QPOs. There have been other attempts also to understand the hard X-ray spectral state variations (Esin et al.,

1997; Titarchuk et al., 2007; Motta et al., 2009; Dunn et al., 2011a,b) as well as state transitions across the HID (Meyer et al., 2007; Meyer-Hofmeister et al., 2009) of the outbursting BH sources. But none of these models, addressed as a whole the issues of evolution of low frequency QPOs as well as soft and hard X-ray spectral components, and spectral state changes across the HID during the entire outburst. On the other hand, quite independently, several alternative models (see §4 for discussion) and more recently the phenomenological model (Fender et al., 2004, 2009) have been put forward only for understanding the disk-jet symbiosis in BH sources.

So, we attempted to understand the evolution of temporal and spectral properties associated with the different branches of the ‘q-diagram’ of the outburst of the source XTE J1859+226 within a single framework of the Two Component Advective Flow (TCAF) model (Chakrabarti & Titarchuk, 1995). Basically, this model consists of two different types of accreting flow (Chakrabarti & Titarchuk, 1995): sub-Keplerian (i.e., freely falling and less viscous flow) and Keplerian (i.e., moves in circular orbit and high viscous flow) matter (Shakura & Sunyaev, 1973). We also delve deep into the nature of the accretion dynamics during the Jet ejections of this source based on the detailed temporal and spectral X-ray properties.

In general, outbursting black hole sources show signature of evolution of QPO frequencies (Belloni & Hasinger, 1990; Belloni et al., 2005; Debnath et al., 2008; Nandi et al., 2012), which could be explained based on the Propagating oscillatory shocks solution (Chakrabarti et al., 2008, 2009; Nandi et al., 2012) of TCAF model. In this work, we provided the solution of evolution of QPOs during the rising phase and possible explanation of the ‘reverse’ nature of the evolution of the hard spectral component (i.e., the fold energy), which can be interpreted with the shock acceleration mechanism (Chakrabarti & Mandal, 2006) in the sub-Keplerian flow. Our findings show that the QPOs are not observed during the radio flares, which we have explained with the possible scenario of ‘evacuation/disruption’ of the Comptonized corona. We attempt to estimate the mass of the source by modeling the QPO evolution and also from the correlation between QPO frequency and photon index (Shaposhnikov & Titarchuk, 2007). The preliminary results of our findings were presented in Nandi & Radhika 2012.

This paper has been organized in the following manner: In the next section, we discuss the observations and the procedures applied for data analysis using the standard packages for RXTE PCA/HEXTE. In §3, we presented the results obtained from the temporal and spectral analysis for the whole outburst, estimation of mass in §3.2, followed by specific spectral and temporal characteristics during each radio flare in §3.3. In §4, we discuss the possible physical scenario to explain the evolution of X-ray properties observed during the entire outburst of XTE J1859+226 and the disk-jet connection, and summarize our conclusions.

## 2. Observation and Data Analysis

We analysed the public archival data obtained from the HEASARC database for the RXTE satellite to study the characteristics of the source XTE J1859+226 over the entire duration of the single outburst which occurred during the entire RXTE era. We analysed the PCA (2 - 25 keV) and HEXTE (20 - 150 keV) data spanning 166 days since October 9, 1999 (MJD 51460.76) to March 23, 2000 (MJD 51626.6). We excluded the observations of July 2000 when the source was in quiescence, as the counts were very less. The standard FTOOLS package of HEASOFT v 6.11 was used for data reduction. For spectral and temporal analysis purposes, we used the packages XSPEC v 12.7 and XRONOS v 5.22 respectively.

For the timing analysis, we used the Science data of PCA in the Binned mode (B\_8ms\_16A\_0.35\_H\_4P, FS37\*) of maximum time resolution of 8 ms which spans over 0 - 35 channels, and Event mode (E\_16us\_16B\_36\_1s, FS3b\*) of 16  $\mu$ s time resolution for 36 - 249 channels. We used the FTOOLS task *xtfilt* to create filter file, and *maketime* to generate a good time interval (*gti*) file, with conditions of *elevation angle > 10°*, *offset of < 0.02* and *time since SAA passage < 30 min*. Since it was not possible to select the data only for a single PCU from the Binned mode data, we decided to extract light curves for all PCUs. Light curves were generated in various energy bands of 2 - 6 keV, 6 - 13 keV, 13 - 25 keV and 2 - 25 keV in order to perform an energy dependent study of the PDS. Since the Binned mode data consisted of only 0 - 35 channels (2 - 13 keV), we generated the light curve of minimum binning time, for the channel ranges 0 - 15 (2 - 6 keV) and 15 - 35 (6 - 13 keV), using *saextract*. The light curve from the Event mode data was created using *seextract* for the minimum available binning time, and the data belonging to channel range of 36 - 67 (13 - 25 keV) was extracted from the total available channel range of 36 - 249. A combined light curve for 2 - 25 keV was obtained, by summing up the light curves from 0 - 35 channels (2 - 13 keV) and 35 - 67 channels (13 - 25 keV), using *lcmath*. Since the contribution of background counts were very less (8.6 counts over 2674 source counts at the peak of the outburst and 6.6 counts over 61.9 source counts at the minimum), we did not subtract the background counts while generating the light curve.

For the spectral analysis, we decided to extract data for PCU2 only, since throughout the entire outburst only PCU2 remained ‘ON’ and the efficiency of the detector also holds good. The source spectra were extracted from the Standard2 data product (FS4a\*), which has a time resolution of 16 sec. Background spectra were obtained with the help of *runpcabackest*, applying the background model for bright source and SAA passage history file obtained from the PCA background web-page<sup>1</sup> of RXTE for the corresponding epoch during which the source has undergone outburst. Spectral response was created using the

<sup>1</sup>[http://heasarc.gsfc.nasa.gov/docs/xte/pca\\_bkg\\_epoch.html](http://heasarc.gsfc.nasa.gov/docs/xte/pca_bkg_epoch.html)

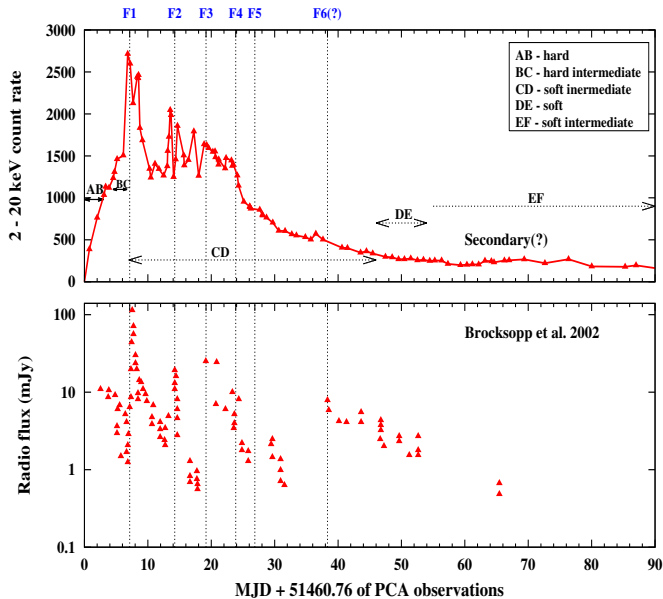


Figure 1: 2 - 20 keV light curve from PCU2 data is shown in the top panel followed by the radio light curve (Brocksopp et al., 2002) in the bottom panel. We also mark the five flares *peak* as F1, F2, F3, F4, F5. Please see text for flares F5 and F6(?) as there were no radio observation during F5 and before F6. The different spectral states (except the hard intermediate (FG) and hard states (GH) in declining phase) are also shown.

*pcarsp* tool. We also generated the background subtracted light curve for PCU2 counts for the energy range 2 - 6 keV, 6 - 20 keV and 2 - 20 keV, in order to plot the HID.

We extracted high energy (20 - 150 keV) spectral data mostly from cluster A (FH52\*) of HEXTE, since specific observation by cluster B (FH58\*) had lesser counts, except for initial two days (MJD 51462.76 and MJD 51463.83), where there were no cluster A observation. Using standard procedures, we generated the deadtime corrected source and background spectra, and spectral response was generated using *hxtresp*.

Radio observations were carried out in the bands of 1.43 GHz, 1.66 GHz, 2.25 GHz, 3.9 GHz by various observatories (VLA, MERLIN, GBI, RATAN) during the outburst of the source, and the combined radio light curve was presented in Brocksopp et al. 2002. We re-produced the radio light curve presented in Brocksopp et al. 2002 using the software ‘DEXTER’<sup>2</sup>. Figure 1 shows the X-ray and the radio light curve for the source XTE J1859+226 during the entire outburst.

Brocksopp et al. 2002 (bottom panel of Figure 1) identified five radio flares during the entire outburst. The five flares were observed to have their *peak* radio flux on MJD 51467.90 (F1), 51475.00 (F2), 51479.94 (F3), 51484.62 (F4), 51487.63 (F5).

<sup>2</sup><http://dexter.edpsciences.org/Dexterhelp.html>

## 2.1. Timing analysis

To obtain the PDS from the lightcurves generated, we used the ‘powspec v 1.0’ of the XRONOS package and the customized software based on IDL, *General High energy Aperiodic Timing Software* (GHATS) v 1.0.1<sup>3</sup>. While using ‘powspec’, a normalisation factor of ‘-2’ was applied in order to subtract the expected white noise level from the data, to obtain the squared rms fractional variability from the integral of the PDS. Further analysis shows that the factor of ‘-2’ deviates about 0.5% in almost all states except the soft-intermediate states where it deviates by 3% to 5%. The GHATS package considers dead time effect and hence the correct value of normalisation factor (as in Zhang et al. 1995) while generating the PDS. The available minimum time binning factor of 0.0078 sec, which corresponds to a Nyquist frequency of 64 Hz, was chosen over 8192 segments. The power obtained in the PDS has units of  $\text{rms}^2/\text{Hz}$ .

We modeled the power spectra from 0.1 to 64 Hz, by different components of *Lorentzians* (Belloni et al. 2002) for the QPOs and broad-band noise, and a powerlaw for the red noise, wherever required. The resultant centroid frequency is considered as the QPO frequency. We also estimated the Q-factor (centroid frequency/width of the Lorentzian), amplitude in rms and significance of the QPO observed. The standard QDP/PLT command of *statistic* was used to obtain the integrated value (rms) for the QPO and for the overall PDS, in the range of 0.1 to 64 Hz. The error values on each parameter of the components were estimated at 90% confidence interval, using the *fit err* command.

We also studied the evolution of PDS in different branches of HID of the outburst. The phase lag between soft (2 - 6 keV) and hard (6 - 25 keV) photons during the flares was estimated using GHATS. The lightcurves and hence the Fast Fourier Transforms for the 2 - 6 keV and 6 - 25 keV energy bands are generated. The cross spectrum is computed, taking into account the subtraction of Poissonian noise (as per Zhang et al. 1995). We followed the standard procedures of the GHATS package to estimate the lag (see also Casella et al. 2004 & Figure 15 of this work).

## 2.2. Spectral analysis

We performed a simultaneous fit of the PCA and HEXTE data for the energy range of 3 - 150 keV, including a constant factor close to unity for normalising both the spectra. In order to get an idea of the normalising factor we estimated the factor by simultaneously fitting the Crab spectra (since it does not vary with time) observed by RXTE during the different spectral states of XTE J1859+226 (observation IDs 40093-01-12-00 and 40093-01-15-00). The constant was observed to be  $\sim 1$ . A simultaneous fit to the PCA and HEXTE spectra of XTE J1859+226 showed that when the constant factor was fixed at 1 for PCA, a

<sup>3</sup>[http://www.brera.inaf.it/utenti/belloni/GHATS\\_Package/Home.html](http://www.brera.inaf.it/utenti/belloni/GHATS_Package/Home.html)



value varying between 0.9 and 1.1 (over the entire data set) was obtained for the constant factor corresponding to HEXTE spectra, which was used during the fitting.

We modeled the energy spectra using the standard accretion disk models (*diskbb* and *powerlaw*) for BH spectra, modified by the *phabs* model to account for the interstellar absorption. From an initial fit to the data sets during the entire outburst, we found that the  $nH$  parameter has an average value of  $0.2 \times 10^{22}$  atoms  $\text{cm}^{-2}$  and fixed this value for further analysis. This value of  $nH$ , agrees well with the average value of  $0.216 \times 10^{22}$  atoms  $\text{cm}^{-2}$ , estimated by the Leiden/Argentine/Bonn (LAB) survey, and the Dickey & Lockman (DL) survey value of  $0.221 \times 10^{22}$  atoms  $\text{cm}^{-2}$  (4). Markwardt 2001 quoted a slightly higher value of  $1.1 \times 10^{22}$  atoms  $\text{cm}^{-2}$ . We find that a change in  $nH$  from 0.2 to 1.1, does not significantly change the overall results.

For an initial fit to the observation 40124-01-11-00 with the model *phabs\*(diskbb+powerlaw)const*, we obtained  $\chi_{red}^2$  ( $=\chi^2/\text{dof}$ ) of 145.43/82. This resulted in residuals around 6.4 keV along with a smeared edge of  $\sim 8$  keV (Ebisawa et al., 1994) and the model considered was *phabs(diskbb+gauss+smedge\*powerlaw)const*, which resulted in  $\chi_{red}^2$  of 64.55/77. The width of the Gaussian was fixed at 0.7 keV (varies between 0.62 keV and 0.88 keV) which was obtained as an average to all the fits (except for the hard states). Systematic error of 0.5% was included in all the fits, for considering the uncertainties in the data. We obtained the parameters of disk temperature, disk normalization, photon index with the powerlaw norm and the line energy of the Gaussian line. The photon index of the HEXTE component was tied to that of the PCA component. Since the combined spectra showed a cut-off feature in the residuals at higher energies, we decided to include a *highecut* model for considering this. The fits improved with  $\chi_{red}^2 = 57.57/75$  for the model of *phabs\*(diskbb+gauss+smedge\*powerlaw\*highecut)*. The F-test probability for inclusion of *highecut* model for this observation is 0.014, but for the observations during the rising phase of the outburst the F-test probability is of the order of  $10^{-28}$  to  $10^{-14}$  implying that inclusion of *highecut* model is statistically significant. We have considered the *highecut* model in order to understand the evolution of the cut-off and fold energy during the spectral states, although the F-test probability for inclusion of *highecut* during the soft-intermediate state is high. Figure 2 shows the unfolded spectrum for the fits using *highecut* model for one of the observations. Hence, it was decided to consider *phabs\*(diskbb+gauss+smedge\*powerlaw\*highecut)* as the final model, and similar method of analysis was followed for all the data sets during the entire outburst.

We also attempted to model the spectrum with *compTT* (Titarchuk, 1994) to take into account the parameters related to the non-thermal component of the spectra (Comptonized corona), and obtained  $\chi_{red}^2 = 72.59/78$  for the

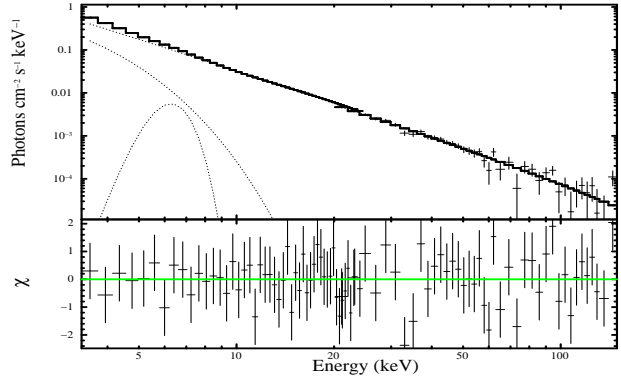


Figure 2: Unfolded PCA (3 - 20 keV) and HEXTE (20 - 150 keV) spectra of the X-ray observation of 24 hrs before the occurrence of first flare (MJD 51466.89, observation ID: 40124-01-11-00). The combined spectra of 3 - 150 keV is modeled by a *diskbb* ( $T_{in} = 0.89$  keV), *powerlaw* ( $\Gamma = 2.35$ ), a high energy cutoff ( $E_{fold} = 151.28$  keV) along with Gaussian & smedge components.

same observation ID. Although the fit for the model *phabs\*(diskbb+gauss+smedge\*compTT)* was statistically good, the variations seen in the parameters were not able to explain the nature of the spectral evolution. We observed that as the source rise towards the peak, the optical depth varied from 1.5 to 0.01, and the seed photon temperature reduced from 2.5 to 0.49 which seems to be unrealistic, although the electron temperature increased from 29 keV to 239 keV.

Recently Farinelli et al. 2013 have performed the spectral analysis of the source in the context of a complex bulk motion comptonization model. In order to have a comparative study, we also applied the model of *wabs\*(diskbb+gauss+bmc\*highecut)const* to the same observation ID, and obtained  $\chi^2/\text{dof} = 93.83/77$ . A comparison with the analysis performed by Farinelli et al. 2013 shows that the fit will probably improve if the BeppoSAX data is also included. In spite of the fact that we did not consider the BeppoSAX data, we studied this model for the different spectral states, and found that the variation of the parameters characterising the disk properties were similar to those shown in Figure 4 of Farinelli et al. 2013. We also found that the value of parameters related to the disk and the photon index obtained using the model we have applied and that used by Farinelli et al. 2013 are within  $1\sigma$  error limit.

Since MJD 51486.87 ( $\sim 26^{th}$  day) to the end of the outburst, the HEXTE spectrum was found to be mostly background dominated (few cases spectra up to  $\sim 50$  keV). Hence, we decided to fit only the 3 - 25 keV PCA spectrum using *diskbb* and *powerlaw*. Better fits were obtained with the model of *phabs(diskbb+gauss+smedge\*powerlaw)* with  $\chi^2/\text{dof}$  of 28.62/39 (for observation ID: 40124-01-40-01).

It is to be noted that since we are considering RXTE data  $\gtrsim 3$  keV only, the value of inner disk temperature obtained from the fits will not be exact. Merloni et al. 2000 pointed out that the *diskbb* model parameters should not

<sup>4</sup><http://heasarc.nasa.gov/cgi-bin/Tools/w3nh/w3nh.pl>

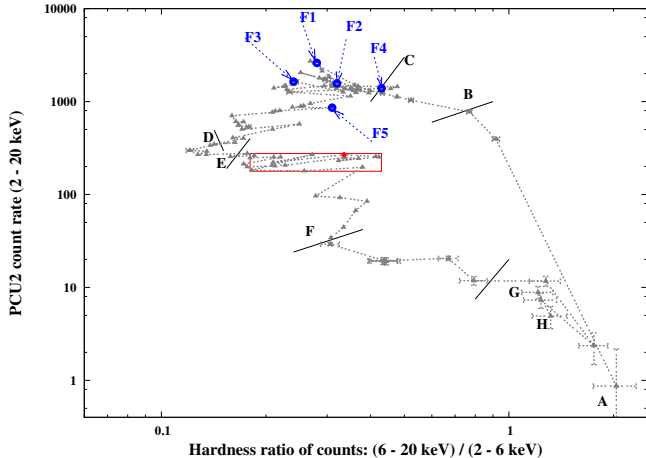


Figure 3: Hardness Intensity Diagram (HID) for the source XTE J1859+226 during the 1999 outburst showing variation of background subtracted count rate with the color, which has been observed with RXTE/PCA (i.e., PCU2). The points marked A  $\rightarrow$  H depict the start/state transitions/end of the outburst. The five flares (F1  $\rightarrow$  F5) observed along with the weak signature of secondary outburst phase (marked as rectangular box) are also shown. See text for details.

be considered as ideal, since the parameter of disk radius varies due to the change in spectral hardening factor (see also Dunn et al. 2011b).

The convolution model, *cflux* was included to find the flux contribution of the individual components, in the energy range of 3 - 150 keV. The error values for each parameter were obtained using the *err* command at a confidence interval of 90%. We observe that the uncertainty in flux estimated using *cflux*, is not of large variation, except a few cases of the soft-intermediate state where a 5% variation is observed. The variation between the values obtained by *cflux* and *flux* commands are found to be a maximum of 4%.

### 3. Results and Modeling

In this section, we present the evolution of temporal and spectral properties (in broad spectral band of 3 - 150 keV) associated with different branches of HID of the source XTE J1859+226 to understand the accretion dynamics from a theoretical point of view. We estimate mass of the source by modeling the QPO evolution and also by correlation studies, and describe the X-ray features observed during the Radio flares and thereby investigate the disk-jet symbiosis.

#### 3.1. Outburst evolution

In this sub-section, we present the characteristics of the HID along with variation of X-ray and Radio flux. Figure 1 shows the intensity variations of the emission from the source, both in X-rays and radio. We observe that as the source rises from quiescence, the background subtracted X-ray Count rate (2 - 20 keV) rises from  $\sim 1$  count/sec

(MJD 51460.76 = 0<sup>th</sup> day) to a peak of 2714 counts/sec (MJD 51467.58). Although for the first observation, the source count rate is very less with large error bars, this observation is important to follow the evolution of the source since the beginning of the outburst. Similar values were quoted by previous studies carried out by Homan & Belloni 2005 and Casella et al. 2004. The radio flux peaks (MJD 51467.9) at a value of 114 mJy resulting in peak flare F1, implying the release of matter in the form of jets (Brockspopp et al., 2002). Multiple ejections have been observed resulting in flare F2 on MJD 51475 at 19 mJy when X-ray intensity was 2045 counts/sec (on MJD 51474.28), flare F3 on MJD 51479.9 at 31 mJy during which the X-ray intensity was 1637 counts/sec, flare F4 at a peak flux of 5.2 mJy on MJD 51484.6 where the X-ray intensity is around 1391 counts/sec. The source count rate starts decreasing from 1444 counts/sec (after MJD 51483.94) to  $\sim 4.9$  counts/sec (MJD 51626.6 = 166<sup>th</sup> day) and attains quiescence. While decaying, the source is observed to show a weak secondary emission (see §3.1.5) for around 24 days with peak emission on 69<sup>th</sup> day (MJD 51530.13) of the outburst. A fifth flare (F5) is reported by Brockspopp et al. 2002 based on ASM lightcurve to occur on MJD 51487.6, but there were no radio observations on that day.

Figure 3 shows the HID (see also Homan & Belloni 2005; Dunn et al. 2011a) plotted using the background subtracted PCU2 count rate. The points where the five flares occurred are also marked in the figure (see also Fender et al. 2009). The possible transitions which occurred, are labelled from A to H. In general, outbursting sources undergo state transitions from *hard*  $\rightarrow$  *hard-intermediate*  $\rightarrow$  *soft-intermediate*  $\rightarrow$  *soft*  $\rightarrow$  *soft-intermediate*  $\rightarrow$  *hard-intermediate*  $\rightarrow$  *hard* (Homan & Belloni, 2005; Belloni et al., 2005; Belloni, 2010; Nandi et al., 2012) and finally into a quiescent state.

In Figure 4, we show the variation of QPO frequency, QPO rms, the Q-factor and significance of the QPOs observed, over the entire outburst of the source XTE J1859+226. The QPO frequencies increase monotonically from 0.46 Hz to 6.09 Hz in the rising phase of the outburst, which is a quite natural phenomena as observed in other outbursting BH sources (Belloni & Hasinger, 1990; Belloni et al., 2005; Nandi et al., 2012). In the later phase of the outburst, the presence/absence of QPO frequencies are directly linked with Jet emission (see Figure 4 and §3.3) as well as with the ‘secondary’ emission of the outburst (see Figure 1 and §3.1.5).

Evolution of the parameters of the spectral fit, obtained from the analysis are shown in Figures 5, 6 and 7. Figure 8 depicts the variation of disk flux and powerlaw flux in the 3 - 20 keV range and also for the 20 - 150 keV powerlaw flux; and Figure 9 shows the fraction of thermal flux contributing to the total 3 - 20 keV flux, the contribution of thermal flux over non-thermal flux (3 - 20 keV) and also that of the flux ratio in 3 - 20 keV to 20 - 150 keV energy range (up to MJD 51486.82).

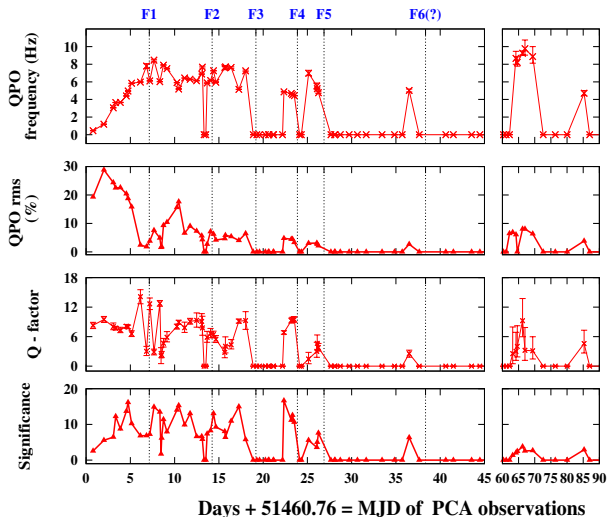


Figure 4: Evolution of QPO frequency, QPO-rms, Q-factor and significance throughout the outburst of XTE J1859+226. Absence of QPOs during radio flares (ejections) are shown in the plot. Peak timings (in unit of days) of Radio flares are also marked as F1, F2, F3, F4 & F5 (see Table 2 for details).

### 3.1.1. Hard state (branch AB)

During the first PCA observation (point A in Figure 3), the PDS was dominated by broad-band noise. The next observation (on MJD 51461.54) has a red noise along with a QPO of 0.46 Hz (Q-factor = 8.31, significance = 2.6, rms amplitude = 19.3%) which was not reported by Casella et al. 2004, and is marked as the first point in the top panel of Figure 4, Figure 10 and Figure 11. Figure 4 implies that the QPO frequency starts rising from 0.46 Hz to 1.19 Hz (type C QPOs; see Casella et al. 2004 for details) with the power spectra being mostly dominated by red noise and the rms of PDS varies from 30% to 24%. This variation in total rms is similar to that observed in other BH sources like GX 339–4 (See Munoz-Darias et al. 2010). In this branch, the photon indices of the energy spectra rise from 1.6 to 2.0, the disk temperature ( $T_{in}$ ) varies in-between 1.01 keV to 0.83 keV (Figure 5) and hard X-ray flux dominates over the disk flux (Figure 8); and the hard X-ray spectral component (i.e., fold energy) increased from 53 keV to 114 keV.

### 3.1.2. Hard-intermediate state (branch BC)

In this branch, the power spectrum has a flat top noise along with QPOs and a powerlaw form at frequencies  $> 10$  Hz, with the total rms varying from 24% to 16% and the QPO frequency increasing from 3.05 Hz to 5.97 Hz (Type C; see Casella et al. 2004). The photon index increases from 2.0 to 2.4 and the disk temperature slowly increases from 0.75 keV to 0.85 keV. The disk flux is observed to be increasing as compared to the non-thermal powerlaw flux (Figure 8), as well as the contribution of low energy to high energy powerlaw flux increases (Figure 9).

Figure 6 shows that during branch BC, the fold energy

increased from 108.3 keV to 201.2 keV. Thus we observe an increase in fold Energy from 53 keV to 201.2 keV, when the source moves through the branches AB and BC during the rising phase. Farinelli et al. 2013 reported about an increase in the cut-off component during the transition from the hard to soft state.

### 3.1.3. Soft-intermediate state (branch CD)

During the initial phase of the branch CD (from MJD 51468.4 to MJD 51473.82), the steepness of the red noise component starts decreasing and the power spectra has a flat top noise along with QPOs (both A and B types). QPOs of type C and also type B *Cathedral or twin QPOs* (Casella et al. 2004) are observed during this branch. QPOs observed after MJD 51484.276 have not been classified into any types (Casella et al. 2004). The total rms of the PDS is observed to increase from 7% to 14%, while during the end phase of the branch (after MJD 51484.87), the PDS has only broadband noise of amplitude 6% to 3% rms, with or without QPOs along with a powerlaw form from 10 Hz to 64 Hz.

The fold energy is observed to vary randomly in-between 64 keV and 180 keV, around an average of 130 keV within  $1\sigma$  error bars (except few data points, which are within  $1\sigma$  to  $2\sigma$ ). The disk flux is seen to vary randomly, whereas the power-law flux decreases gradually as shown in Figure 8. During the later phase of this state, the disk temperature slightly decreases from 0.85 keV to 0.7 keV and photon index decreases from 2.4 to 2.0 (Figure 7). Although Farinelli et al. 2013 has reported a photon index of 1.8 during the period of MJD 51490 to 51501, we observed a photon index varying between 1.9 and 2.4 with disk flux contribution of  $>65\%$ . These parameters imply the characteristics of a soft-intermediate state during this period and not a hard state as suspected by Farinelli et al. 2013.

During this state, multiple ejection events have occurred and observed in Radio as flares (Brocksopp et al., 2002). Fender et al. 2009 has reported on the features of HID and temporal characteristics during a flare. We present detailed observational results of the spectral and temporal properties, during each of these flares in §3.3.

### 3.1.4. Soft-state (branch DE)

During the transition from branch CD, we find that a few of the observations (MJD 51504.31 to MJD 51510.29 in Figure 1) show hardness ratio around 0.1 (Figure 3) and total rms  $\sim 1\%$  to  $2\%$ , which suggest a short presence of soft state (see Munoz-Darias et al. 2010). Similar value of hardness ratio was quoted in Figure 19 of Casella et al. 2004, Figure 1 of Homan & Belloni 2005 and Figure A.1 of Dunn et al. 2011a, for this source. During these observations the thermal flux dominates the spectra (see top panel of Figure 9) and QPOs are also not observed. But the other spectral features during this phase seems not to imply the characteristics of the ‘canonical’ soft state as suggested by McClintock & Remillard 2006. We observe that as compared to branch CD (soft-intermediate state),

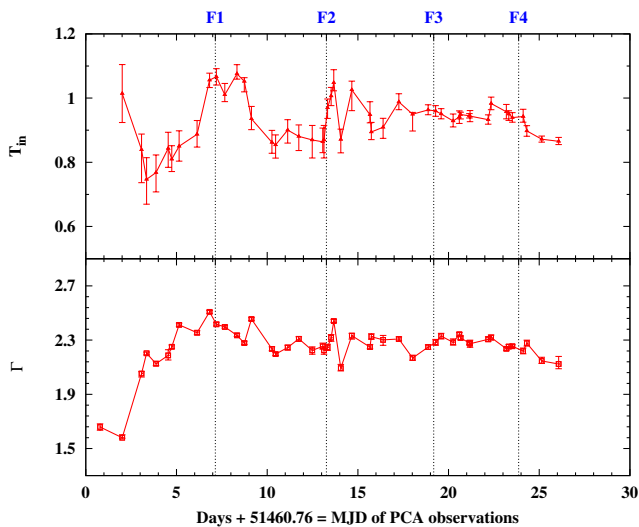


Figure 5: Evolution of the spectral parameters, *disk temperature* ( $T_{in}$ ) and *photon index* ( $\Gamma$ ) of observations before flare 5 (F5) of the source XTE J1859+226.

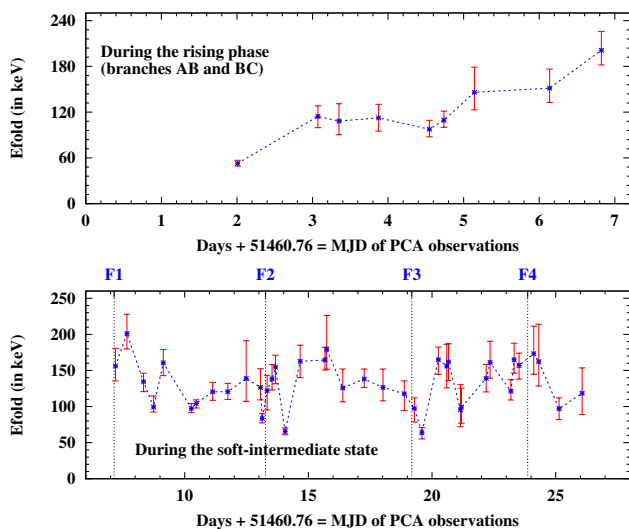


Figure 6: Evolution of fold Energy ( $E_{fold}$ ) during the rising phase (branches AB, BC; top panel) and soft-intermediate state (branch CD; bottom panel) of the HID for the source XTE J1859+226.

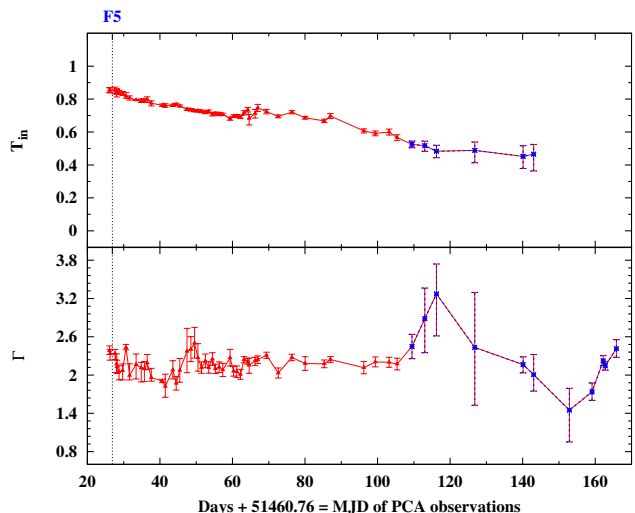


Figure 7: Evolution of the spectral parameters (3 - 25 keV energy range), *disk temperature*  $T_{in}$ , *photon index*  $\Gamma$  for observations from flare 5 (F5) till the end of the outburst of XTE J1859+226. Note, spectral data is fitted up to 15 keV (around 120<sup>th</sup> day) during the unusual variation of photon index.

the disk temperature reduces from 0.9 keV to 0.7 keV (to be noted that it is not the exact value, due to the limitations of RXTE and diskbb model (Merloni et al., 2000)) and the photon index remains  $\sim 2.2$  (spectra are harder compare to soft-intermediate state). These variations are very different from the observations of other BH sources where the disk temperature remains high above 1 keV, photon index is  $>2.5$  during the soft state (See §4.3.5 and Figures 4.8 and 4.9 in McClintock & Remillard 2006; Belloni et al. 2006). All these results deviate from the ‘canonical’ description of soft spectral state observed in outbursting BH sources (Belloni et al., 2005, 2006; McClintock & Remillard, 2006; Belloni, 2010).

### 3.1.5. Soft-intermediate state (branch EF)

In branch EF, no significant QPOs are observed (Casella et al. 2004 has not classified the QPOs also), and the PDS has broadband noise of rms value  $\sim 3\%$ . The source is in the declining phase and we observe that the disk and power-law flux start gradually decreasing (Figure 8) without any signature of hard X-ray flux beyond 50 keV.

- The outburst profile (top panel of Figure 1, see also Figure 3) indicates that, during this phase there is an enhancement in X-ray flux (also observed by RXTE-ASM) and it gradually decreases to the quiescence. From the spectral analysis, we observed that there is an increase in the disk and powerlaw flux (Figure 8) along with increase in disk temperature for  $\sim 24$  days i.e., from 63<sup>rd</sup> to 87<sup>th</sup> day of the outburst (Figure 7 and Figure 1). Although the value of inner disk temperature ( $T_{in}$ ) is less, we note that the variation in uncertainty of  $T_{in}$  is less than the value of  $T_{in}$  itself (see also McClintock & Remillard



Table 1: Details of temporal characteristics during the ‘secondary’ outburst

MJD	Day	QPO frequency (Hz)	Significance of QPO	QPO rms (%)	Q-factor
51523.941	63.18	0	0	0	0
51524.940	64.18	$8.66^{+0.8}_{-0.6}$	2.04	6.87	$3.02^{+3.8}_{-1.8}$
51525.353	64.59	$8.21^{+0.6}_{-0.4}$	2.48	6.03	$4.02^{+4.2}_{-2.1}$
51527.004	66.24	$9.25^{+0.2}_{-0.1}$	3.75	8.02	$9.24^{+4.5}_{-3.2}$
51527.736	66.97	$9.75^{+0.9}_{-0.7}$	2.56	8.03	$3.23^{+4.6}_{-2.0}$
51530.133	69.37	$8.86^{+0.7}_{-1.1}$	2.66	6.32	$3.11^{+2.8}_{-1.6}$
51546.036	85.27	$4.71^{+1.2}_{-0.3}$	2.90	3.82	$4.58^{+2.7}_{-1.9}$
51547.766	87.00	0	0	0	0

2006). The increase in disk and powerlaw flux can also be noted in Figure 14 of Dunn et al. 2011a, after  $\sim$  MJD 51530. Although such an increase in flux has been observed in other sources like GX 339–4 (Dunn et al., 2011a), but that particular observation ( $\sim$  MJD 52710) was associated with the hard-intermediate state (Belloni et al., 2002; Motta et al., 2011). The temporal analysis for the source XTE J1859+226 indicates weak signature of QPOs in the PDS, during this phase of branch EF for the days from 64<sup>th</sup> to 85<sup>th</sup> of the outburst as shown in Figure 4 (see also Casella et al. 2004). Table 1 which summarizes the details of temporal features during this phase, implies the presence of QPOs. QPOs of significance  $\gtrsim 2.7$  (with higher Q-factor) are observed during MJD 51527.004, MJD 51530.133 and MJD 51546.036. Other QPOs seem to be weak (significance  $\sim 2.5$ ) in nature (except the QPO observed on MJD 51523.941 with significance of  $\sim 2$ ), but having Q-factor  $\sim 3$ . Since the source is in the declining phase of the outburst, these QPOs observed can be classified as type C\*. Both the spectral and temporal properties seem to suggest that probably this phase/feature could be associated with a ‘secondary’ emission, within the same outburst.

As the source approaches the end phase of branch EF, there is a sudden increase in the photon index from 2.2 to 3.2 (spectral data fitted up to 15 keV), but with large errors (star points in Figure 7), which turns out to be a puzzling nature.

It is observed that during both the soft-intermediate branches CD and EF, there are QPOs of types A, B, and a few C and C\* (see also Casella et al. 2004).

### 3.1.6. Hard-intermediate state (branch FG)

In branch FG, we do not observe any QPOs and the power spectra remain to have broadband noise with total amplitude (rms) varying from 7% to 11%. The source is in the declining phase and the spectra is dominated by powerlaw component, although we find weak signature of thermal flux with reduced inner disk temperature.

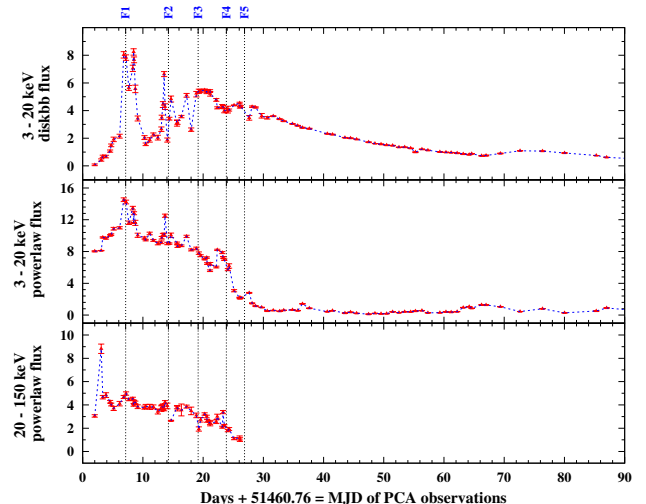


Figure 8: Variation of the flux contribution by the disk component and powerlaw component in the energy range of 3 - 20 keV, and 20 - 150 keV powerlaw flux. Flux values are quoted in units of  $10^{-9}$  erg  $\text{cm}^{-2}$   $\text{s}^{-1}$ .

### 3.1.7. Hard state (branch GH)

At the end of the outburst, the source finally moved towards the hard state, which has characteristics similar to branch AB. The amplitude (rms) of the power spectrum has increased to  $\sim 25\%$  without any signature of QPOs. The energy spectra are mostly powerlaw in nature with photon index around 1.4 except during the last three observations which show a photon index of  $\geq 2.1$  although the source count rates are very less with large errors, and it was difficult to fit the spectra.

## 3.2. Modeling of QPO frequency evolution and $\Gamma$ - QPO correlation

### • QPO evolution

The evolution of QPO frequencies during rising phase of XTE J1859+226 can be understood based on the Propagating Oscillatory Shock (POS) solution (Chakrabarti et al., 2008, 2009; Nandi et al., 2012; Debnath et al., 2013) of the TCAF. According to this model, the oscillating frequencies observed as QPOs are due to the movement of the shock surface (i.e., Comptonizing region). During the rising phase, the shock moves towards the BH and during the declining phase it moves away from the BH. The POS solution states that the QPO frequency is inversely proportional to the infall time scale, and the QPO frequency ( $\nu_{QPO}$ ) can be obtained with a knowledge of the instantaneous shock location or vice-versa, and from the value of the compression ratio ( $R = \rho_+/\rho_-$ , where  $\rho_+$  and  $\rho_-$  are the densities in post and pre shock flows). According to Ryu et al. 1997, Chakrabarti & Manickam 2000, the frequency of the shock location is similar to the observed QPO frequency. Thus, the QPO frequency for an axisymmetric toroidal bounded

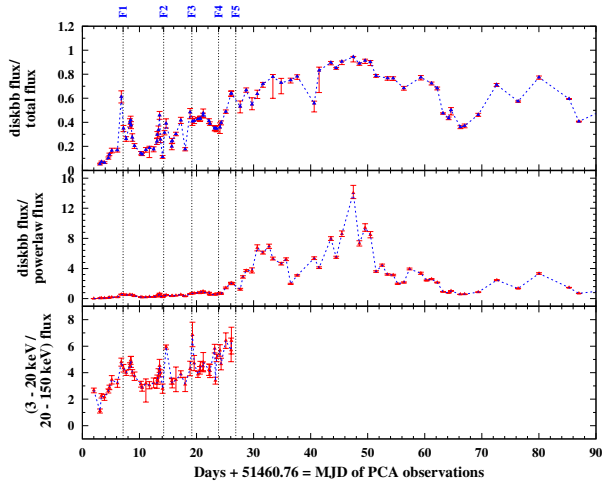


Figure 9: Variation of the fraction of disk flux over the total flux, fraction of disk flux over powerlaw flux in the energy range of 3 - 20 keV, and of the ratio in 3 - 20 keV to 20 - 150 keV flux. Flux values are quoted in units of  $10^{-9}$  erg  $\text{cm}^{-2}$   $\text{s}^{-1}$ .

system (i.e., shock surface; see Figure 18) can be written as

$$\nu_{QPO} = \frac{\nu_{s0}}{t_{infall}} = \frac{\nu_{s0}}{[2\pi R r_s (r_s - 1)^{1/2}]}, \quad (1)$$

where  $\nu_{s0} = c/r_g$  is the inverse of the light crossing time of the BH, and  $r_g = 2GM/c^2$  for a BH of mass  $M$ . Since the shock will be drifting with time (Chakrabarti et al., 2008, 2009), the time dependent shock location can be expressed as

$$r_s(t) = r_{s0} \pm v_0 t / r_g, \quad (2)$$

where  $r_{s0}$  is the shock location at time  $t=0$  and  $v_0$  is the corresponding shock velocity (Chakrabarti & Manickam, 2000; Molteni et al., 1996). The '+' sign is used for an outgoing shock in the declining phase and the '-' sign is used for an inward shock during the rising phase.

In Figure 10, we show the evolution of QPO frequency with time (days) during the rising phase of XTE J1859+226, which we modeled using above equations of the POS solution. Fitted result allows to calculate the shock location and hence to estimate the size of the Comptonizing region. Similar attempts have been performed for GRO J1655-40, XTE J1550-564 (Chakrabarti et al., 2008, 2009), GX339-4 (Nandi et al., 2012) and H 1743-322 (Debnath et al., 2013).

The first day of PCA observation is considered as  $t=0$  sec. Figure 10 shows that the initial three observations of QPOs follow one trend while the rest

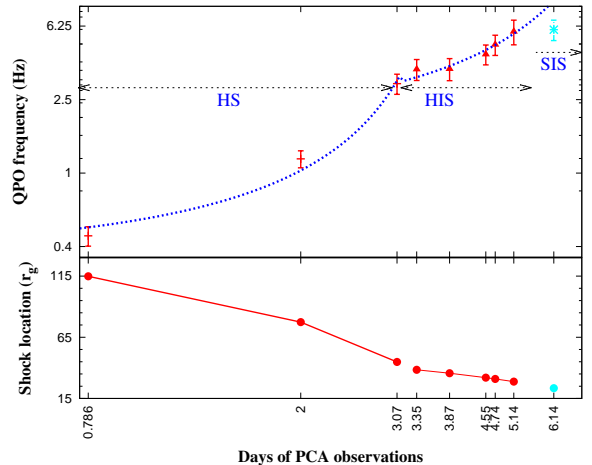


Figure 10: Evolution of QPO frequencies with days, during the rising phase of the outburst of XTE J1859+226. The FWHM of the fitted Lorentzian of the QPO has been considered as the error bars. The curves show the fitted solution based on the POS model. The spectral states (HS: Hard state, HIS: hard-intermediate state, SIS: soft-intermediate state) has also been marked. The bottom panel shows the variation of the shock location (i.e., Comptonizing region; See also §4 for discussions on the same).

shows another. Hence the evolution follows two different solutions for different parameters of shock location, velocity etc.. The FWHMs obtained from the fits to the Lorentzian feature of the QPOs have been considered as error bars. The fit to the initial three QPO frequencies gives the value of compression ratio as  $R=3.8$ , initial shock location  $r_{s0}$  of  $138.8 r_g$  ( $t=0$  sec) and the shock velocity  $v_{s0} = 8.5 \text{ ms}^{-1}$ . The fit to the rest of the QPO frequencies during the rising phase gives  $R=3.2$ ,  $r_{s0}=56.5 r_g$ ,  $v_{s0}=1.5 \text{ ms}^{-1}$ . The overall fit yields a mass of BH of  $7.12 \pm 0.54 M_{\odot}$ , with reduced  $\chi^2$  of 0.69.

In the final fitting, we excluded the last observation (as shown in cyan color) on MJD 51466.89, which is just before the first radio flare (F1). The variation of shock locations (i.e, the size of Comptonizing region) is shown in the bottom panel of the Figure. The oscillation of shock stalled at  $21.2 r_g$  and this gives the estimate of minimum size of the comptonizing region (before the flare F1). From Figure 10, it can be observed that there is a kink (see also Chakrabarti et al. 2009; 1998 outburst of XTE J1550-564) at the point where the two fitted functions meet.

#### • $\Gamma$ - QPO correlation

Based on the model developed by Titarchuk & Fiorito 2004, Shaposhnikov & Titarchuk 2007 found that a correlation exists between the QPO frequency and photon index for BH sources. They found that the correlation can be explained by the function

$$f(\nu) = A - DB \ln(\exp(\frac{\nu_{tr} - \nu}{D}) + 1) \quad (3)$$

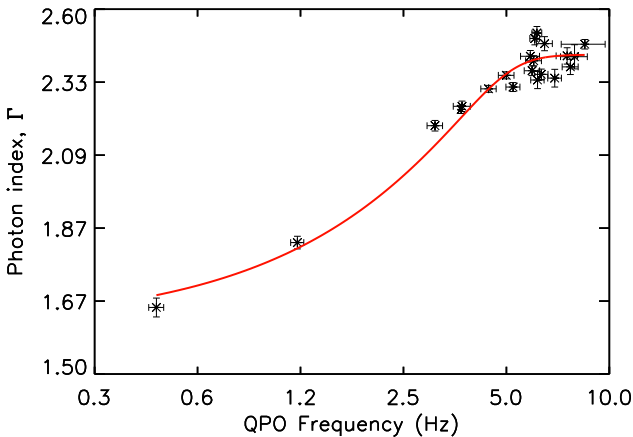


Figure 11: Correlation of  $\Gamma$  and QPO frequency during the rising phase of the outburst (before F2) of XTE J1859+226. The FWHM of the fitted Lorentzian of the QPO has been considered as the error bars.

by scaling w.r.t a source which has similar evolution. The above correlation is linear with a slope for lower frequencies, and nearer to a particular frequency  $\nu_{tr}$  it becomes constant. The parameter A denotes the value of the index saturation level, B is slope of the low-frequency part of the data and D controls how fast the transition occurs.

In Figure 11, we have shown the correlation of photon index and QPO frequency for the source XTE J1859+226.

Similar studies was performed by Shaposhnikov & Titarchuk 2009 and the mass of the source XTE J1859+226 was estimated as  $7.7 \pm 1.3 M_{\odot}$ . In our analysis, we have considered the observation results of MJD 51461.54, which was not reported in Shaposhnikov & Titarchuk 2009, and those during the rising phase of the outburst. We performed the scaling w.r.t GRO J1655–40, since the evolution of photon index of XTE J1859+226 saturates  $\sim 2.4$ , which is closer to that of GRO J1655–40 at 2.3, as mentioned in Shaposhnikov & Titarchuk 2007. GRO J1655–40 is also a well studied source with a dynamical mass estimate of  $6.3 \pm 0.5 M_{\odot}$ . The value of D was fixed at 0.6 Hz. The fit was performed by applying Craig Markwardt’s IDL routines of *mpfit* (Markwardt, 2009), considering the errors in  $\Gamma$  and QPO frequencies. The resultant fit parameters obtained were  $A_{1859} = 2.427 \pm 0.008$ ,  $B_{1859} = 0.168 \pm 0.008 \text{ Hz}^{-1}$  and  $\nu_{tr} = 4.84 \pm 0.18 \text{ Hz}$ . Thus from the relation

$$M_{1859} = B_{1859} \times (M_{1655}/B_{1655}),$$

we obtained the mass of the source XTE J1859+226 as  $7.96 \pm 0.88 M_{\odot}$ , where  $B_{1655} = 0.133 \pm 0.008 \text{ Hz}^{-1}$ .

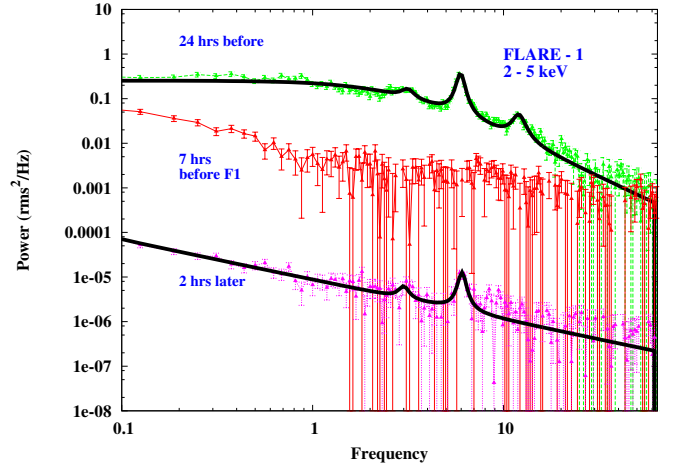


Figure 12: Variation of the PDS implying that the QPO is not observed in the energy range of 2 - 5 keV, during the first flare (F1). The power shown in y-axis has been scaled by a factor of 100, 1 and 0.1, from the top to bottom. Similar variations also observed in the power spectra of 13 - 25 keV band.

### 3.3. ‘Spectro-temporal’ characteristics of the source during the flares

In this section, we present the results based on the variations of temporal and spectral features during radio flares i.e., when the jet ejections have taken place to understand the disk-jet symbiosis. In Table 2, we summarize the properties of the source during the flares. As mentioned in §2, we have performed an energy dependent study of the PDS (in the bands 2 - 6 keV, 6 - 13 keV and 13 - 25 keV) of all the observations, in order to understand the nature of the X-ray features during the flares.

#### 3.3.1. FLARE - I (F1)

The X-ray observation  $\sim 24$  hrs before (MJD 51466.896) the radio flare peak on MJD 51467.9, shows the presence of a type C QPO of 5.97 Hz. For the next observation (MJD 51467.581) which is 7 hrs before the flare peak we performed energy dependent study in narrower bands (2 - 4 keV, 2 - 5 keV, 2 - 6 keV etc.) and found that the power spectra for 2 - 5 keV and 13 - 25 keV bands does not show any signature of QPO. A broad 7.79 Hz type A QPO is observed, only above 5 keV as evident in the 6 - 13 keV PDS with rms amplitude of 3%, which is typical for type A QPOs. So, in the overall range of 2 - 25 keV, a broad QPO of 7.79 Hz is observed (see also Casella et al. 2004). The next observation which is 2 hrs after the flare peak, shows a type B QPO of 6.1 Hz in all the energy bands. We also observe that the total rms of the PDS reduces (see also Fender et al. 2009) to a value of 2.7% when the QPO is not observed. Since the QPO was not observed in the soft band of 2 - 5 keV, we have shown the variation in the PDS over 2 - 5 keV in Figure 12, for observations before and after the flare peak. Similar variations in the power spectra of 13 - 25 keV band also observed (not shown in Figure).

Table 2: Details of X-ray properties (in 2 - 25 keV band) of the observations during all the flares

X-ray/Radio	X-ray Flux	MJD	Date	Time	Radio flux	QPO				$\Gamma$	$T_{in}$
(ID/Flare)	(cts/sec)				(mJy)	frequency(Hz)	rms(%)	sig.	type		(keV)
40124-01-11-00 <sup>b</sup>	1505	51466.896	1999-10-15	21:30:08		5.97±0.02	15.4	6.83	C	2.35 <sup>+0.01</sup> <sub>-0.02</sub>	0.88 <sup>+0.04</sup> <sub>-0.05</sub>
40124-01-12-00	2714	51467.581	1999-10-16	13:57:20 (7 hrs) <sup>a</sup>		0	0	0	-	2.51±0.01	1.05±0.02
<b>F1</b>		51467.904	1999-10-16	21:41:45.6	114						
40124-01-13-00 <sup>c</sup>	2597	51467.961	1999-10-16	23:04:16		6.1±0.02	3.8	7.24	B	2.42 <sup>+0.02</sup> <sub>-0.01</sub>	1.07±0.02
40124-01-23-01 <sup>b</sup>	1558	51473.890	1999-10-22	21:22:08		7.6 <sup>+0.11</sup> <sub>-0.09</sub>	4.3	5.82	C*	2.22 <sup>+0.02</sup> <sub>-0.03</sub>	0.87±0.05
40124-01-15-02	1726	51474.087	1999-10-23	02:06:40		7.3±0.3 †	5.4	5.75	C*	2.25±0.02	0.97±0.03
40124-01-15-03	2045	51474.287	1999-10-23	06:54:40		0	0	0	-	2.32±0.03	1.00±0.03
40124-01-24-00 <sup>c</sup>	1984	51474.429	1999-10-23	10:18:08		5.87±0.07	2.7	7.36	B	2.44 <sup>+0.02</sup> <sub>-0.01</sub>	1.04 <sup>+0.04</sup> <sub>-0.02</sub>
40124-01-25-00	1248	51474.820	1999-10-23	19:41:20 (6 hrs) <sup>a</sup>		6.14±0.04	7.1	8.27	C	2.09 <sup>+0.03</sup> <sub>-0.02</sub>	0.87 <sup>+0.03</sup> <sub>-0.05</sub>
<b>F2</b>		51475.0	1999-10-24	00:00:00	19						
40124-01-31-00 <sup>b</sup>	1262	51478.777	1999-10-27	18:39:28		7.24 <sup>+0.08</sup> <sub>-0.09</sub>	6.4	5.76	C*	2.16 <sup>+0.02</sup> <sub>-0.01</sub>	0.94 <sup>+0.04</sup> <sub>-0.05</sub>
40124-01-32-00	1637	51479.635	1999-10-28	15:15:28 (7 hrs) <sup>a</sup>		0	0	0	-	2.24 <sup>+0.02</sup> <sub>-0.01</sub>	0.96 <sup>+0.01</sup> <sub>-0.02</sub>
<b>F3</b>		51479.940	1999-10-28	22:45:07.2	31						
40124-01-33-01	1625	51480.044	1999-10-29	01:04:32		0	0	0	-	2.28±0.02	0.96±0.01
40124-01-36-00 <sup>c</sup>	1474	51483.106	1999-11-01	02:33:20		4.87±0.04	4.7	16.6	B	2.32±0.01	0.98±0.02
40124-01-37-02 <sup>b</sup>	1391	51484.275	1999-11-02	06:37:20 (8 hrs) <sup>a</sup>		4.43±0.02	3.3	10.6	B	2.25±0.01	0.94±0.01
<b>F4</b>		51484.625	1999-11-02	15:00:35.8	5.2						
40124-01-38-00 <sup>b</sup>	1266	51484.872	1999-11-02	20:56:16		0	0	0	-	2.21 <sup>+0.03</sup> <sub>-0.02</sub>	0.94±0.02
40124-01-39-00 <sup>c</sup>	952	51485.874	1999-11-03	20:59:44		6.97 <sup>+0.4</sup> <sub>-0.2</sub>	3	5.56	C* <sup>e</sup>	2.14 <sup>+0.03</sup> <sub>-0.02</sub>	0.87±0.01
40124-01-41-00 <sup>b</sup>	870	51487.009	1999-11-05	00:13:36 (15 hrs) <sup>a</sup>		4.77 <sup>+0.07</sup> <sub>-0.08</sub>	2.1	7.59	C* <sup>e</sup>	2.34±0.1	0.85 <sup>+0.01</sup> <sub>-0.02</sub>
<b>F5<sup>d</sup></b>		51487.63	1999-11-05	15:15:23.1	-						
40124-01-42-00	857	51488.41	1999-11-06	09:49:36		7.39 <sup>+1.1</sup> <sub>-0.7</sub> †	3.1	1.3	C* <sup>e</sup>	2.33 <sup>+0.07</sup> <sub>-0.09</sub>	0.84±0.02
		51488.48	1999-11-06	11:31:28		7.34 <sup>0.39</sup> <sub>-0.34</sub>	3.1	4.5	C* <sup>e</sup>		
40124-01-43-00	765	51489.47	1999-11-07	11:27:28		0	0	0	-	2.05 <sup>+0.09</sup> <sub>-0.07</sub>	0.85±0.02
40124-01-49-00	502	51496.462	1999-11-14	11:06:24		0	0	0	-	2.10±0.02	0.79 <sup>+0.01</sup> <sub>-0.02</sub>
40124-01-49-01 <sup>c,b</sup>	571	51497.254	1999-11-15	06:06:40		5.02±0.08	2.7	6.32	C* <sup>e</sup>	2.18 <sup>+0.14</sup> <sub>-0.1</sub>	0.79±0.02
40124-01-50-01	502	51498.390	1999-11-16	09:22:24 (16 hrs) <sup>a</sup>		0	0	0	-	1.96 <sup>+0.05</sup> <sub>-0.06</sub>	0.77 <sup>+0.01</sup> <sub>-0.02</sub>
<b>F6 (?)</b>		51499.100	1999-11-17	02:24:00.0	7.9						
40124-01-51-00	406	51501.384	1999-11-19	09:13:36		0	0	0	-	1.90 <sup>+0.03</sup> <sub>-0.02</sub>	0.76±0.01

Absence of QPO during F1 (in 2 - 5 keV and 13 - 25 keV band), whereas QPOs were absent in 2 - 25 keV during all other flares. **a** - minimum duration of X-ray observation before flare; **b** - observation of last QPO before flare; **c** - observation when QPO reappeared; **d** - No Radio observations, flare day based on ASM light curve (Brocksopp et al., 2002), radio flare might have occurred after this (see Figure 1); **e** - Not classified in Casella et al. 2004; † - weak indication



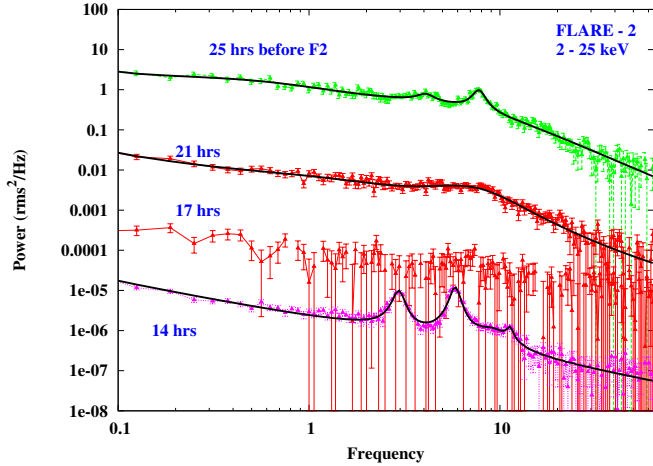


Figure 13: Evolution of the PDS in the energy range of 2 - 25 keV during the 2nd flare (F2). Absence of QPO is seen  $\sim$  17 hrs before the radio flare peak of F2. The power spectra are scaled by factor of 1000, 10, 1, 0.01 from top to bottom.

It is seen that, before the flare occurred i.e., when the QPO was observed, the hard photons slightly lag behind the soft photons. 7 hrs before the flare peak, the 2 - 5 keV soft photons are lagging compared to 5 - 25 keV hard photons. When the QPO is observed again in the PDS, the hard photons are observed to lag the soft photons.

We also note that before the flare peak, the photon index increased to 2.51, disk temperature increased from 0.88 keV to 1.06 keV (Table 2 and Figure 5) and the fold energy of the electrons increased from 151 keV to 201 keV. The disk flux increased from  $2.14 \times 10^{-9}$  erg cm $^{-2}$  s $^{-1}$  to  $8.03 \times 10^{-9}$  erg cm $^{-2}$  s $^{-1}$  (Figure 8) and dominated over the powerlaw flux (3 - 20 keV) by a factor of 0.55. The 3 - 20 keV flux is found to be more than the 20 - 150 keV flux, by a factor of 5 (Figure 9), suggesting the soft nature of the spectrum. This implies that the emission is disk dominated.

After the flare, the photon index decreased to 2.42 and disk flux reduced to  $7.83 \times 10^{-9}$  erg cm $^{-2}$  s $^{-1}$ . This implies the hard nature of the spectrum although the disk temperature was around 1.07 keV and the fold energy had reduced to 156 keV.

Thus the broad QPO seen (just 7 hrs before the flare peak) in the 6 - 13 keV band while not in 2 - 5 keV and 13 - 25 keV, implies that the QPO is ‘partially’ observed (see also Markwardt 2001). We could not observe a ‘complete absence of the QPO’ (i.e., in 2 - 25 keV band) due to lack of continuous X-ray observations during the flare and just before/after. The spectrum also softens as compared to the spectrum of the observation before the flare.

### 3.3.2. FLARE - II (F2)

Radio observation shows that the flare F2, peaked on MJD 51475.0 with a flux of 19 mJy. 25 hrs earlier (MJD 51473.89) to the peak of F2, we observe type C\* QPOs in the PDS. The observations  $\sim$ 21 hrs before (MJD 51474.087)

peak of F2 shows a weak signature of QPO with an increase in frequency (7.3 Hz with Q-factor of 1.2, significance of 5.75). 4 hrs later (MJD 51474.287) the PDS of F2 shows complete absence of QPOs and the total rms reduces to 3.02% (see also Fender et al. 2009). Cathedral B-type QPOs are observed at frequencies 3 Hz & 6.1 Hz in the next X-ray observation which is 14 hrs before (MJD 51474.429) peak of F2. The evolution of power spectra is shown in Figure 13, which clearly indicates the ‘absence’ of QPO during the flare, but QPO is observed again before the flare peak (see §4 for discussion).

We find that when the QPO is not significant in the power spectra, the soft photons are lagging. 17 hrs before peak of flare F2 where there is a complete absence of QPO, no lag of soft to hard photons is seen. When the QPO is observed again,  $\sim$ 14 hrs before peak of F2, the hard photons are observed to lag behind the soft photons.

The corresponding softening of the spectra is also observed in the variation of the spectral parameters. When the QPO was not present (over MJD 51473.89 to MJD 51474.287), we noted that the disk temperature increases from 0.87 keV to 1 keV, and the photon index also increased from 2.22 to 2.32. The disk flux increased from  $2 \times 10^{-9}$  erg cm $^{-2}$  s $^{-1}$  to  $7 \times 10^{-9}$  erg cm $^{-2}$  s $^{-1}$  (Figure 8), but the fold energy increased from 83 keV to 138 keV. The ratio of disk flux over powerlaw flux increased from 0.43 to 0.65 with a significant decrease in hard X-ray flux (Figure 9). When the QPO was observed again, the photon index further increased to 2.44, with the disk temperature  $\sim$  1 keV only. The disk flux reduced to  $\sim$   $4.28 \times 10^{-9}$  erg cm $^{-2}$  s $^{-1}$ , whereas the fold energy increased to 154 keV. This suggest that, the nature of variation in spectral features along with the temporal properties (i.e., QPO features) during F2, is different from that of flare F1 and hence disk-jet symbiosis could be further complex (see §4 for discussions).

### 3.3.3. FLARE - III (F3)

On MJD 51478.777, a 7.2 Hz type C\* QPO is observed. Radio observations indicate that multiple flares (see Figure 1) have occurred on MJD 51479.94 within  $\sim$  40 hrs of gap with flux values of 31 mJy & 24 mJy during the period when F3 occurred. The X-ray observation which is around 7 hrs before F3, does not show any signature of QPO and the PDS is dominated by broad-band noise component (Figure 14). The subsequent X-ray observations does not show QPOs and the total rms decreased (see also Fender et al. 2009) to 2.4%. QPOs are observed almost after 3 days at a frequency of 4.8 Hz (type-B).

We find an indication of soft photon lagging just before the flare peak, whereas when the QPO is not at all observed ( $\sim$  3 days), no lag is observed. The hard photons are observed to be lagging, when the QPO is observed again after 3 days (see Figure 15).

During F3, disk temperature and photon index increases slightly, whereas the soft flux increased from  $2.2 \times 10^{-9}$  erg cm $^{-2}$  s $^{-1}$  to  $5.2 \times 10^{-9}$  erg cm $^{-2}$  s $^{-1}$  (Figure 8),

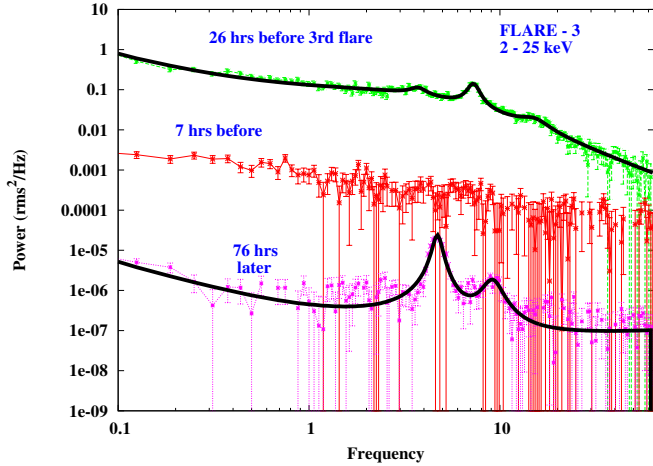


Figure 14: Evolution of the PDS in the energy range of 2 - 25 keV during the flare F3. QPOs are absent  $\sim$  7 hrs before the radio flare peak of F3. The power spectra are scaled by factor of 100, 10, 0.01 from top to bottom.

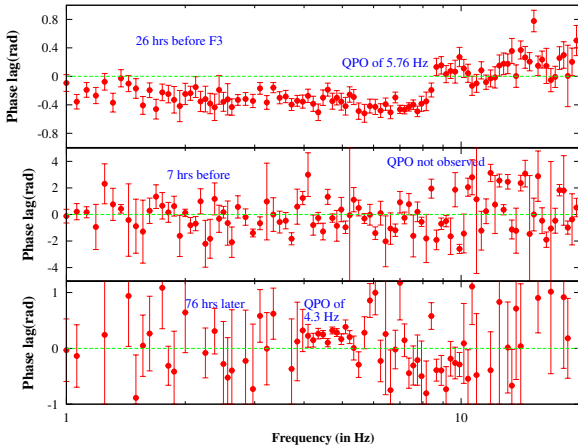


Figure 15: The variation in phase lag between 2 - 6 keV and 6 - 25 keV, during the occurrence of flare F3. No phase lag is observed when QPO is not observed in the PDS.

which implies the softening of the spectra. The fold energy decreased from 126 keV to 97 keV. We also note that during the observations where there were no QPOs, disk flux dominates over the powerlaw flux by a factor of 0.6 to 0.9 with a significant decrease in hard X-ray flux (see bottom panel of Figure 9). At the same time, the power-law index and fold energy varies, but the disk temperature remains almost constant (Figure 5).

The QPOs observed before and after the ejections during the flares F1, F2 and F3 are of type C/C\* and type B respectively (see Table 2).

### 3.3.4. FLARE - IV (F4)

Around 8 hrs before (i.e. on MJD 51484.27) the peak of next flare F4, a type B QPO is observed. The subsequent observations (on MJD 51484.87 and MJD 51485.07) does not show any signature of QPOs (Figure 4), except

broadband noise in the PDS (power spectral evolution not shown here) with decreased total rms of 2.5% which is consistent with Fender et al. 2009. It is also clear from Figure 1 that a flare has occurred with a flux of 5.2 mJy (MJD 51484.625). Brocksopp et al. 2002 reported the time of flare based on X-ray observation from ASM. 6 hrs after the peak of F4 (MJD 51484.87), QPOs are completely absent in the power spectra and are observed only after 30 hrs (on MJD 51485.874) at a frequency of 6.97 Hz (type C\* with less rms and less Q-factor; see Casella et al. 2004 for details of type C\* QPOs).

During the flare F4, soft photons are observed to be lagging, while in flares F2 and F3, no lag of soft to hard photons was observed.

It is also seen from Figure 5 and Table 2 that during the flare peak, the spectral index varied around 2.2. The disk temperature remained around 0.9 keV, whereas the fold energy varied around 150 keV (Figure 5). The ratio of low energy to high energy flux increases with a factor of  $\sim$  6 (lower panel of Figure 9), implying the nature of spectral softening. The disk flux dominated over the non-thermal flux by a factor of 0.57 to 0.71, as seen in Figure 9. When the QPO was observed again, the photon index decreased to 2.14, with inner disk temperature of  $\sim$  0.87 keV, and decreased fold energy of 96 keV.

### 3.3.5. FLARE - V (F5)

We observe a 4.7 Hz QPO in the PDS of MJD 51487.01. Although the Q-factor is less, these QPOs can be considered as of Type C\* class based on the QPO frequency and amplitude. The next X-ray observation (MJD 51488.41) indicates the presence of a weak QPO at 7.39 Hz (type C\*) in the PDS of MJD 51488.41 and another type C\* QPO at 7.34 Hz on MJD 51488.48. During the observation on MJD 51489.47 QPOs are not observed in the power spectra (see Figure 16). Brocksopp et al. 2002 has reported a ejection/jet (radio flare), to have occurred on MJD 51487.63, based on the X-ray observations by ASM (see also Fender et al. 2009). But there were no radio observations (see bottom panel of Figure 1) during this time. The weak presence of QPO on MJD 51488.41 and MJD 51488.48, was followed by a complete absence of QPO in the power spectra of MJD 51489.47 along with softening of the spectra. This indicates that the fifth radio flare would have probably occurred after the time reported by Brocksopp et al. 2002. This is also implied by the detection of a 2.4 mJy radio flux on MJD 51490.4 (see Figure 1). QPOs (type C\*) are observed only after  $\sim$ 10 days (MJD 51497.25).

Thus during F5 we observe that the QPO observed before and after the flare is of type C\*, whereas during flare F4 the evolution of QPO is from type B to type C\*. These features are not similar to that observed during the flares F1, F2 and F3.

The variation in spectral parameters does not show any significant change during the flare F5. The photon index is

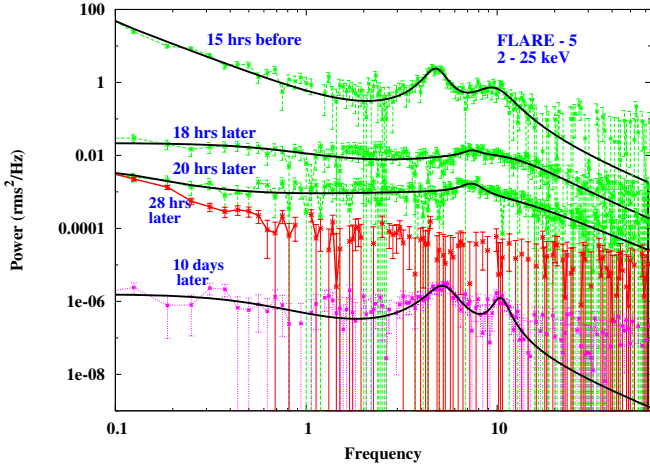


Figure 16: Evolution of the PDS in the energy range of 2 - 25 keV during the flare F5. Scaling factors of 10000, 100, 10, 1 and 0.01 are applied for the power spectra from top to bottom.

seen to vary in between 2.38 and 2.33, while the disk temperature remains almost constant around 0.79. Although the disk flux decreased from  $4.24 \times 10^{-9} \text{ erg cm}^{-2} \text{ s}^{-1}$  to  $\sim 3.48 \times 10^{-9} \text{ erg cm}^{-2} \text{ s}^{-1}$ , the ratio of disk to powerlaw flux is observed to increase by a factor of 3 to 6.7 (top panel of Figure 9) along with significant decrease of hard X-rays photons (beyond 50 keV), implying the softening nature of the spectrum. When the QPO is observed again, the photon index has reduced to 2.18 with the disk temperature of  $\sim 0.79 \text{ keV}$ . The disk flux value is observed to dominate over the non-thermal flux, but with a lesser factor of 1.9.

We observe a signature of QPO (type C\* with lesser Q-factor) at 5.02 Hz (on MJD 51497.25), after 10 days of flare F5. The next observation (on MJD 51498.39) does not show any QPOs (Figure 4) in the PDS, except a broad band noise. The total rms of the PDS reduces from 4.02% to 1.6%. Radio observations also show that the flux decreases to  $\sim 1 \text{ mJy}$  and later the source becomes non-detectable. We find that, there is a radio brightening (see Brocksopp et al. 2002) on MJD 51499.10 (after 16 hrs of X-ray obs.) of flux of 7.9 mJy (Figure 1), implying the possible signature of occurrence of a flare (F6?) that could have triggered on or before this time.

Since the evolution of the different types of QPOs during the ejections seems to be complex, we attempt to understand if any correlation exists between the QPO frequencies of different QPO types, with the thermal and non-thermal flux. The same has been presented in the following sub-section.

### 3.4. Relation between QPO frequency and flux variation

In Figure 17, we show the variation of disk and powerlaw flux as a function of QPO frequency for the observations in hard state (AB), hard-intermediate state (BC) and up to MJD 51484.27 during flare F4 in the soft-intermediate (branch CD) of HID (see Figure 1 & 3), so as to consider

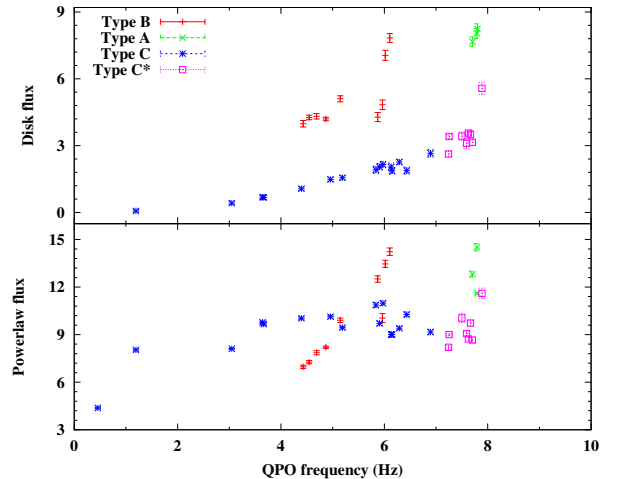


Figure 17: Variation of the disk flux and powerlaw flux with increase in QPO frequency. The flux values are quoted in units of  $10^{-9} \text{ erg cm}^{-2} \text{ s}^{-1}$ .

the types of QPOs which have been already classified in Casella et al. 2004. We observed that during the rising phase (hard and hard-intermediate states) the QPO frequency of type-C increases as both the disk and powerlaw flux increases, implying a positive correlation. During the soft-intermediate state (branch CD) the type B QPOs are observed to be correlated with the powerlaw (non-thermal) flux but not with the disk flux. A few type C QPOs detected during the soft-intermediate state (branch CD) are observed not to show any correlation with the powerlaw flux. Figure 17 also shows that a few of the type C\* QPOs have a correlation with the disk flux but are not at all correlated with the powerlaw flux as indicated by the random variation. Only very few type A QPOs are observed, and hence it is not possible to find any correlation with disk or powerlaw flux.

## 4. Discussions and concluding remarks

The evolution of temporal and spectral properties of the source XTE J1859+226 during the 1999 outburst suggest that the source does evolve via different spectral states throughout the outburst. Detailed analysis during the multiple ejections (i.e., radio flares) reveals that the ejections are possibly associated with the Comptonized corona, and hence the sudden ‘appearance’ of such radio flares or ‘jets’ could be because of some instability happening in the Comptonized corona. Although several attempts have been made to understand the evolution of ‘spectro-temporal’ characteristics as well as the ejection events observed in outbursting BH sources, till date, there is no comprehensive picture for the 1999 outburst of XTE J1859+226.

In this paper, we attempted to understand the possible accretion dynamics associated with the evolution of various X-ray features of XTE J1859+226, in the context of Two Component Advective Flow (TCAF) model



(Chakrabarti & Titarchuk 1995; Giri & Chakrabarti 2013). According to TCAF, the Compton cloud (formed in shocked accretion phase) is nothing but the sub-Keplerian matter dominated CENtrifugal pressure supported BOundary Layer (i.e., CENBOL), which intercepts soft photons, mostly originated from the Keplerian disk, and the CENBOL up-scatters them via inverse Comptonization to produce high energy photons. The CENBOL forms due to shock transition in the flow and its surface may oscillate due to the oscillation of shock, which could be responsible for the generation of QPOs (Molteni et al. 1996; Ryu et al. 1997; Chakrabarti & Manickam 2000; Chakrabarti et al. 2004; Okuda et al. 2007; Lee et al. 2011, see references therein).

During the rising phase, we observed a monotonic increase of QPO frequency (C type) from 0.46 Hz to 5.84 Hz in both hard and hard-intermediate states. This happens because, the shock location propagates towards the BH and the size of the shock formed region i.e., the CENBOL surface or region of Comptonization, (which is oscillating) reduces, and hence the QPO frequency increases (Chakrabarti et al. 2008, 2009; Nandi et al. 2012). We estimated the shock location (size of CENBOL) based on the POS solution (see §3.3). During this period, the instantaneous shock location (see Figure 10) and hence the ‘Compton cloud/CENBOL’ varies from  $114.7 r_g$  to  $28.7 r_g$ . Using the same solution, we also estimated the size of the CENBOL region, before and after the flare.

During the soft-intermediate state, the QPO frequency (all types of QPOs) varies in between 6 Hz to 8 Hz, and this implies that the size of the corona/CENBOL remains almost constant (i.e., shock location varies between  $21.1 r_g$  to  $17.5 r_g$ ). We also found that QPOs in the soft-intermediate state are sporadic in nature i.e. OFF (QPO not observed) and ON (QPO observed again), which could be linked with jet ejection (see Figure 4 and below for discussion). During the declining phase of soft-intermediate (except during the ‘secondary’ emission of outburst), hard-intermediate and hard states, QPOs are hardly observable, whereas for other BH sources like GX 339–4, H 1743–322, XTE J1550–564 QPOs are observed during all the spectral states (except soft states) (Chakrabarti et al., 2009; Nandi et al., 2012; Debnath et al., 2013).

Titarchuk et al. 2007 evoked the idea of the diffusive propagation of perturbation in the disk like configuration of Keplerian (as extended disk) and sub-Keplerian (inner part of the disk as ‘Compton’ cloud) matter distribution (Chakrabarti & Titarchuk, 1995), to understand the different noise component in the power spectra. So, it could be possible to explain the evolution of total rms as well as modeling the broadband power spectra of different branches of HID of XTE J1859+226, in the context of TCAF model, although detailed modeling of evolution of the power spectra of the source is beyond the scope of the present work.

The evolution of the HID (Figure 3) shows that during the rising phase, the source was initially in the hard state

(region AB), and the variation of the spectral parameters, suggest that the spectra is mostly dominated by the sub-Keplerian component (i.e., larger ‘Compton’ cloud) with negligible contribution from the Keplerian disk. As the source moves towards the hard-intermediate state (implied by Figures 3 and 5), we observe that thermal flux increases relatively more than the non-thermal flux (Figure 8) and both are correlated with the increase in frequency of type C QPOs (see Figure 17). This implies that the Keplerian flow starts increasing along with the sub-Keplerian flow, which is still dominating over the Keplerian in the hard-intermediate state (BC of HID). As a result, the energy spectra become softer and the size of the CENBOL also starts decreasing (see Figure 10). This is evident from the increase of QPO frequencies during the hard-intermediate state. It is observed that as the source move from hard to hard-intermediate states, the fold energy also (see Figure 6) increases (increase in cut-off energy during hard to soft transition was observed by Farinelli et al. 2013). The increase in fold energy seems to be quite ‘unnatural’ compared to other BH sources, like GX 339–4 and XTE J1550–564, where Figure 6 of Motta et al. 2009 and Figures 1 and 2 of Titarchuk & Shaposhnikov 2010 respectively, pointed out the monotonic decrease of cutoff energy during the rising phase. It seems that the shock acceleration mechanism, which converts fraction of thermal electron to the non-thermal electron within the Compton cloud, becomes more important as the source evolves in this phase, and hence the fold energy increases although the source spectra becomes softer and softer. Similar kind of behaviour is observed in the hard and soft state spectrum of Cyg X–1, which has been modeled using shock acceleration mechanism in TCAF (Chakrabarti & Mandal, 2006).

It has to be noted that the kink observed around  $3^{rd}$  day during the rising phase (see Figure 10), when the QPO frequency changes from 3.05 Hz to 3.64 Hz, is peculiar in sense that at the same time there is an abrupt change in the photon index from 2.05 to 2.2 along with an increase in disk flux from  $0.42 \times 10^{-9} \text{ erg cm}^{-2} \text{ s}^{-1}$  to  $0.7 \times 10^{-9} \text{ erg cm}^{-2} \text{ s}^{-1}$ . This could be possible due to sudden change in the accretion flow dynamics during this phase.

During the soft-intermediate state (CD & EF) the evolution pattern of HID is complex. We find that the photon index varies in between 2.5 to 2.1 and disk temperature varies around 0.9 keV, whereas variation of diskbb and power-law flux is not at all correlated (see Figure 8). This unnatural variation of flux occurs in short time-scales (few hrs to day scales). Also, the fold energy varies randomly about an average value of 130 keV within  $1\sigma$  error limits, whereas the change in fold energy during rising phase is well above the  $2\sigma$  error limit. This could be due to multiple ejections that have taken place, and they are directly associated with the disk dynamics. We observe all types of QPOs during this phase of which the B-type QPO correlates with power-law flux whereas its variation is random with disk flux and hence no correlation exists. C-type



QPOs are correlated with the disk flux but does not show any specific correlation with the power-law flux. So, it is possible that sub-Keplerian flow plays a major role (to generate various types of QPOs, relation between various types of QPOs with flux) compared to the Keplerian flow, as the ‘hot’ Compton cloud evolves faster (i.e., less viscous) than the Keplerian disk.

We could observe a short presence of a ‘soft state’ during branch DE for a few observations (see Figure 3) where the hardness ratio is of  $\sim 0.1$  and total rms of PDS  $\sim 1\%$  to  $2\%$  without any signature of QPO. During this phase, the Keplerian flow is supposed to dominate over the sub-Keplerian flow to produce ‘softest’ spectrum. As observed, the energy spectra is dominated by thermal emission (see Figure 9) but harder in nature (disk temperature also less) compared to the soft-intermediate state (see Figure 5 and 7). Hence, the observed state could not be a ‘canonical’ soft state. This could be possible due to enhancement of sub-Keplerian flow during this time that makes the spectra harder along with the strong presence of Keplerian flow (i.e., thermal emission). It can be understood in the context of TCAF model that, the multiple ejections during the soft-intermediate state restrict the disk to become Keplerian dominated flow since the ejections are coupled with the Comptonized corona, which is mostly sub-Keplerian in nature.

While the source continued in the soft-intermediate state (branch EF), there is an indication of weak increase in X-ray intensity (‘secondary’ emission) of around 24 days with peak emission on 69<sup>th</sup> day of the outburst (see Figure 1). The monotonic increase in QPO frequencies (see Figure 4) and increase in other spectral parameters (Figure 7, 8 and Table 1; see also Dunn et al. 2011a), indicate that there could have been sudden increase in Keplerian as well as in sub-Keplerian flow during the declining phase of the outburst, which results as a weak ‘secondary’ emission. The weak presence of soft state and the weak ‘secondary’ emission, makes the HID different from the ‘standard’ evolution pattern of other outbursting sources (Homan & Belloni 2005; Belloni et al. 2005; Belloni 2010; Mandal & Chakrabarti 2010; Nandi et al. 2012).

At the end of the outburst, the source transits from soft-intermediate to hard via hard-intermediate state before reaching the quiescence phase. The photon index starts decreasing, with a very weak signature of thermal emission (Figure 7 and 8), which implies that the emission component is again dominated by sub-Keplerian matter over Keplerian matter.

The modeling of the HID (i.e., q-track, see also Mandal & Chakrabarti 2010; Nandi et al. 2012) which follows the evolution of X-ray features of the outburst, and of the broadband spectrum (3 - 150 keV) will be carried out using TCAF model and will be presented elsewhere (Nandi et al. (in prep.)).

Results of the modeling (see §3.2) of QPO evolution based on POS solution and  $\Gamma$ -QPO correlation suggest that the mass of the source is  $\sim 6.58$  to  $8.84 M_{\odot}$ . This

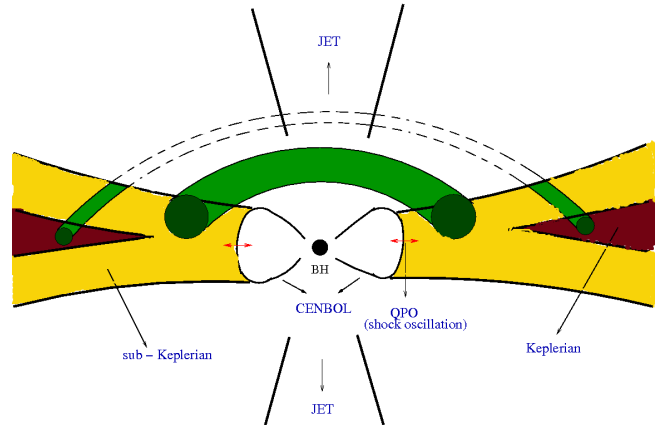


Figure 18: A pictorial representation of the magnetised-TCAF model, showing both the Keplerian and sub-Keplerian flows along with the toroidal magnetic flux tube and jet emission. (Adopted from Chakrabarti & Titarchuk 1995; Nandi et al. 2001). See Giri & Chakrabarti 2013 for simulation of TCAF model.

matches well with the previous estimate of the mass as  $7.7 \pm 1.3 M_{\odot}$  by Shaposhnikov & Titarchuk 2009.

The sudden occurrence of a radio flare can be due to some disturbance in the disk system, which results in ejection of the material as jets. Several attempts have been made until now, to explain the phenomena of jet ejection in BH binaries (see also Fender et al. 2009). Study of the jet emissions, using MHD simulations were carried out by Meier & Nakamura 2004, McKinney & Gammie et al. 2004 and De Villiers et al. 2005. These models suggest that the corona is like a windy hot material which blows away as jets from the inner regions of the accretion flow. In this work, we attempted to explain the ejection mechanism based on dynamics of magnetic flux tube inside the TCAF (see Figure 18) as described by Nandi et al. 2001.

When the ejection takes place due to the collapse of magnetic flux tube, the CENBOL gets disrupted and the matter is ejected as a jet. As a result, oscillation of the CENBOL (i.e., shocked surface) ceases and hence, the QPOs will not be observed in the PDS. The energy spectra shall be dominated by thermal emission from the disk, as the matter from the CENBOL (‘hot’ electron) is ejected. The fold energy is observed to increase just before the flare and decrease just after the flare. This could be the possible indication of ‘disruption’ of the corona/CENBOL. The subsequent observation of QPO and spectral hardening in a time scale of few hours to days suggest that the matter flows in sub-Keplerian disk forming the Compton cloud/CENBOL responsible for QPO generation.

As the observations suggest that the companion is of K-type (Corral-Santana et al., 2011) and hence magnetically active, it is possible that the strong magnetic field anchored with the matter is continuously fed into the disk system during the rising phase of the outburst. Hence, during the transition from hard to soft-intermediate state, the field gets sheared and stronger (in the form of toroidal flux tube) and disrupts the Comptonized corona (in differ-

ent time scales), resulting in multiple ejections at different time-scales.

For the flare F1, we observe a type C QPO of 5.97 Hz which corresponds to a CENBOL size of  $21.2 r_g$ . During the partial absence of the corona (i.e., QPO is not observed in 2 - 5 keV and 13 - 25 keV bands)  $\sim 7$  hrs before the flare peak, we observe a 7.79 Hz QPO at a shock location of  $17.8 r_g$ . Since the sub-Keplerian flow moves in shorter time scale it takes less duration of time to form the CENBOL again, which starts oscillating. Hence QPO of 6.1 Hz (type B) is observed 2 hrs after the flare peak at a shock location of  $20.9 r_g$ . Thus, a duration of 9 hrs (maximum) was required for the CENBOL to get disrupted and form again.

During flare F2, a 7.7 Hz type C\* QPO is observed at  $17.9 r_g$  around 21 hrs before the flare peak. But within 7 hrs, the sub-Keplerian component (as the flow is less viscous) has formed the corona and the oscillations of 5.87 Hz (type B) are re-stored at  $21.4 r_g$ . A closer look into the PDS evolution (Figure 13) shows that the QPO frequency increases with diminishing power, before the flare occurs and the QPO is not observed (see §3.3.4). The QPO was again observed before the radio flare peak, which seems to be inconsistent as compared to other flares, where we observe a complete absence of QPO before the radio peak. We observe similar characteristics in other sources like XTE J1550–564, where the time gap between QPO being not observed and the flare peak was more than 24 hrs (Radhika et al. (in prep.)). So, it is possible that the process of evacuation of the CENBOL is rather slow during F2, and hence the ejected material took long time to peak as a radio flare. By that time, the corona is formed again to reproduce the QPOs, which are interestingly of *Cathedral type*. As we mentioned, the QPO and Jet formation are coupled with the Comptonized corona, which is sub-Keplerian in nature. Hence, the disk-jet coupling mechanism in F2, which seems to be ‘complex’ in nature (‘spectro-temporal’ properties are totally different from other flares) could be because the dynamics (i.e., the amplification of magnetic field, motion of tube etc.) of flux tube within the CENBOL are different. It requires further investigation to study the coupling between flux tubes and sub-Keplerian flow and hence to understand the ‘complex’ disk-jet symbiosis. But, for both the flares F1 and F2, the disruption of the inner part of disk and its re-filling time required for oscillation of CENBOL, is around 7 to 9 hrs. So, it is evident that within the hours time-scale only the sub-Keplerian matter can easily move in, whereas the Keplerian flow does not since it moves in viscous time-scale.

Before the peak of flare F3 a 7.24 Hz type C\* QPO is observed corresponding to the CENBOL size of  $18.6 r_g$ . When the QPO is observed again at 4.87 Hz (type B) the shock location is  $24.3 r_g$ . We find that, the disruption and refilling time of the inner disk (formation of oscillating CENBOL) is  $\sim 3$  days. It is possible that the magnetic field would have been strong enough (i.e., continuous collapse of flux tube) to disrupt the disk repeatedly, resulting in multiple signature of radio activity (see bottom panel

of Figure 1). During this long disruption process, no lags in soft to hard photons are observed, disk temperature remains almost constant with increased disk flux and the fold energy decreases. These indicate that the ‘hot’ Compton cloud is ejected in the form of jets. As the source is also in the declining phase, the matter supply in both the form of Keplerian and sub-Keplerian flow has reduced and hence, took longer duration to form the inner-part of the disk for the oscillation of the CENBOL to start again.

During F4, before the flare peak the QPO was observed at 4.43 Hz (type B) and the CENBOL size is of  $25.9 r_g$ . When the QPO is observed again its frequency is 6.97 Hz (type C\*) at  $19.1 r_g$ . Before F5, we observed a significant QPO of 4.7 Hz (type C\*) at  $24.9 r_g$  followed by weak indication of 7.3 Hz QPOs (type C\*) at  $18.2 r_g$ , and after the flare the QPO is again observed with frequency of 5.02 Hz (type C\*) at  $23.8 r_g$ . The flares F4 and F5 occurred when the source was in the declining phase of the outburst, where the sub-Keplerian flow dominates. While in decay the rate of incoming matter (both the Keplerian and sub-Keplerian) from the companion reduces, and hence the strength of the magnetic field also reduces. So, we notice that the radio flares observed have less peak flux as compared to previous flares. Although there are no radio observations during the flare F5 (see Brocksopp et al. 2002; Fender et al. 2009), the results we obtained (§3.3.5) suggest that the flare would have probably occurred after the day reported by Brocksopp et al. 2002. As a result, during both the flares, the disruption and refilling time of inner part of the disk (formation of oscillating CENBOL) is longer of around 30 hrs for F4 (with a possibility of secondary emission after  $\sim 16.8$  hrs with radio flux of  $\sim 8.9$  mJy as shown in Figure 1) and 10 days for F5 respectively.

We found a possibility of occurrence of another radio flare (i.e., F6) on or before MJD 51499.10 with radio flux of  $\sim 7.9$  mJy. There is an indication of QPO not being observed after the peak radio flux. As there is lack of X-ray and radio observations during this time, it is not possible to pinpoint the exact time of flare ejection.

Above discussions on all the flares suggest that the Radio flare take different time to peak and QPOs are not observed during the flares. The re-filling time scale ( $\sim$  few hrs to days based on available data) to form oscillating CENBOL (corona) resulting in QPOs, also suggests that the accretion flow could be sub-Keplerian in nature.

Similar study of the disk-jet connection based on the magnetized TCAF model has been earlier presented for GRS 1915+105 by Nandi et al. 2001; Vadawale et al. 2001.

We observe that the type of QPO is independent of the ejection event (See §3.3 and Column 10 of Table 2). The results mentioned in §3.3 clearly show that the QPOs observed before and after the flare, need not be of specific type. But, the prediction of Jet ejections (without any radio detection), based on QPOs being observed or not in the power spectra, requires further studies in the context of TCAF model which could be possible after detailed investigation of X-ray observation of other outbursting sources.

We have also observed similar characteristics (but with no definite relation between the types of QPOs before and after the ejection) in other BH sources. In the case of XTE J1550–564, GRO J1655–40 and XTE J1752–223, we found that the QPO observed before and after the flare are of type C. For H 1743–322, we observed a type C QPO before the ejection and the PDS showed a type B QPO after the ejection. So, in the present scenario, it is not possible to generalise or establish a relation between types of QPO and flare ejection events. Although, there were attempts to establish the link of B type QPOs with radio flare, along with the drop in rms in the power spectra (see Soleri et al. 2008; Fender et al. 2009). Detailed study on QPO types and radio flares will be performed for several BH sources (based on available X-ray and radio data) (Radhika et al. (in prep.)).

Due to the complex behaviour of QPOs during ejection events, we presented in §3.4 how different types of QPOs are correlated with the flux variations. The variation of type B/C QPOs w.r.t disk and powerlaw flux is not similar to that observed for GX 339–4 by Motta et al. 2011, where both type B and C QPOs are correlated with the disk and powerlaw flux (see Figures 5 and 8 in Motta et al. 2011). Figure 17 also shows that the type C\* QPOs have a weak correlation with the disk flux but does not have any correlation with the powerlaw flux, and a similar characteristic was observed for GX 339–4 by Motta et al. 2011. Type A QPOs do not show any correlation with flux for GX 339–4, while XTE J1859+226 has only very few type A QPOs, which limits the results. Sobczak et al. 2000 and McClintock et al. 2009 observed a positive correlation between QPO frequency and disk flux during the rising phase (for GRO J1655–40, XTE J1550–564, H 1743–322), which is also observed for XTE J1859+226. An opposite correlation was observed between QPO frequency and powerlaw flux for GRO J1655–40, while a positive correlation was observed for XTE J1550–564 and H 1743–322.

In the present work, we have not explained the origin of different types of QPOs before and after the ejections. According to TCAF model, the base of the Jet and origin of QPOs both are directly coupled with the CENBOL dynamics. Recently, we have done simulation to show that the mass loss from the disk and origin of QPOs in BH are linked with the CENBOL (Das et al. 2014, see references therein). So, it could be possible to address the types of QPOs during the ejections, as the QPO generation in TCAF model depends on the sub-Keplerian flow characteristics (i.e., viscosity, angular momentum, energy etc. of the flow). This work which involves detailed simulation (SPH and TVD based) is under progress and would be presented elsewhere.

There have been reports of flare events (radio ejections) during the outburst of sources like XTE J1748–288 (Brocksopp et al. 2007), XTE J1752–223 (Brocksopp et al. 2010) and H 1743–322 (Miller-Jones et al. 2012). The study of the outburst evolution and flaring events associ-

ated with X-ray properties observed for the BH sources XTE J1748–288, XTE J1752–223, H 1743–322, XTE J1550–564, GRO J1655–40, GX 339–4 and MAXI J1836–194, in the context of TCAF model is under progress. Preliminary results on the presence and absence of QPOs associated with flaring events for several outbursting black holes have been presented in Radhika et al. 2013; Nandi et al. 2013.

## 5. Summary

Based on the findings of ‘spectro-temporal’ evolution of the source XTE J1859+226, we can summarize that:

- The source evolved through various states in HID with a sequence of *hard* → *hard-intermediate* → *soft-intermediate* → *soft state (not ‘canonical’)* → *soft-intermediate* → *hard-intermediate* → *hard states* before reaching to the quiescence phase. Multiple radio ejections (or the enhancement in sub-Keplerian flow) might have stopped the source to evolve from soft-intermediate to ‘canonical’ soft state.
- The QPO frequency increases monotonically during the rising phase of the outburst. The evolution is modeled with POS solution to estimate the size of the ‘Compton’ corona. Similar kind of variation is also observed in other outbursting BH sources.
- Results from the modeling of the QPO evolution and  $\Gamma$ -QPO correlation suggest that mass of the source could be between  $6.58 M_{\odot}$  and  $8.84 M_{\odot}$ .
- The temporal evolution of the PDS shows that the QPOs are not observed, during the ejection as observed in radio.
- During F1, no QPO is observed in the soft band of 2 - 5 keV (also not in 13 - 25 keV band), but a broad QPO of less amplitude is observed in the 6 - 13 keV band. This implies that there has been a ‘partial’ absence of the QPO in 2 - 5 keV and 13 - 25 keV bands.
- During F2, F3, F4 and F5, we find that the QPOs are not at all observed in the PDS.
- The QPO frequency observed before and after the flare need not be of same type during all the flares.
- During all the ejections, the X-ray spectrum gets soften and fold energy ( $E_{fold}$ ) decreases, as the ‘hot’ electron cloud (corona) gets disrupted and spectrum is dominated by disk emission. Only in the case of F2,  $E_{fold}$  increases, the evacuation process seems to be complex.
- ‘Disruption’ of inner part of the disk (corona/CENBOL) occurs as a resultant of dominant thermal emission



over non-thermal flux resulting in QPOs being not observed. This could be due to the ‘catastrophic collapse’ of toroidal flux tube of strong magnetic field in the hot region of sub-Keplerian flow.

- During the declining phase, the source might have undergone a ‘secondary’ outburst observed as a weak X-ray flaring activity for  $\sim 24$  days.
- Due to lack of continuous X-ray observation during the flare time, it was not possible to tighten the duration of disruption and refilling time scale. So, it is required to have more precise and simultaneous observation in *radio-UV-X-rays* to provide better picture of disk-jet dynamics in outbursting sources. In this context, continuous monitoring of outbursting sources with India’s upcoming multi-wavelength satellite ASTROSAT along with GMRT, VLBI etc. will be a best opportunity for studying the complex accretion dynamics of BH sources.

## Acknowledgments

We thank Dr. P. Sreekumar (IIA, Bangalore), Dr. S. Seetha (ISRO Headquarters) and Dr. A. Agarwal (ISAC, Bangalore) for various suggestions and support. Radhika D., acknowledges the research fellowship provided by ISRO Satellite Centre.

This research has made use of the data obtained through High Energy Astrophysics Science Archive Research Center on-line service, provided by NASA/Goddard Space Flight Center and of the General High-energy Aperiodic Timing Software (GHATS) package developed by Dr. Tomaso Belloni at INAF - Osservatorio Astronomico di Brera.

We thank Dr. Dipankar Bhattacharya of Inter University Centre for Astronomy & Astrophysics, Pune for providing an opportunity to participate in the ‘Advanced X-ray timing workshop’ and also to Dr. Tomaso Belloni for the sessions on usage of GHATS.

We are thankful to the anonymous referees for their suggestions which helped to improve the manuscript.

## References

### References

Belloni T. M., Hasinger G., 1990, A&A, 230, 103  
 Belloni T. M., Psaltis D., van der Klis M., 2002, ApJ, 572, 392  
 Belloni T. M., Homan J., Casella P., et al., 2005, A&A, 440, 207  
 Belloni T. M., Parolin I., Del Santo M., et al., 2006, MNRAS, 367, 1113  
 Belloni T. M., 2010, ‘The Jet Paradigm - From Microquasars to Quasars’, Lect. Notes Phys 794, edited by T. Belloni, 794, 53  
 Blandford R. D., Znajek R. L., 1977, MNRAS, 179, 433  
 Bradt H. V., Rothschild R. E., Swank J. H., 1993, A&A supplement series, 97, 355  
 Brocksopp C., Fender R. P., McCollough M., et al., 2002, MNRAS, 331, 765  
 Brocksopp C., Miller-Jones J. C. A., Fender R. P., Stappers B. W., 2007, MNRAS, 378, 1111

Brocksopp C., Corbel, S., Tzioumis T., Fender R. et al., 2010, Atel, 2400  
 Cadolle Bel M., Rodriguez J., D’Avanzo P. et al., 2011, A&A, 534, 119  
 Casella P., Belloni T., Homan J., Stella L., 2004, A&A, 426, 587  
 Casella P., Belloni T., Homan J., Stella L., 2005, ApJ, 629, 403  
 Chakrabarti S. K., & D’Silva, S., 1994, ApJ, 424, 138  
 Chakrabarti S.K., Titarchuk L.G., 1995, ApJ, 455, 623  
 Chakrabarti S.K. & Manickam, S.G., 2000, ApJ, 531, L41  
 Chakrabarti, S. K., Nandi, A., Manickam, S., et al., 2002, ApJ, 579, L21  
 Chakrabarti S. K., Acharya K., Molteni D., 2004, A&A, 421, 1  
 Chakrabarti S. K., Mandal S., 2006, ApJ, 642, 49  
 Chakrabarti S. K., Debnath D., Nandi A. & Pal P. S., 2008, A&A, 489, L41  
 Chakrabarti S. K., Dutta B. G., & Pal P. S., 2009, MNRAS, 394, 1463  
 Corral-Santana J. M., Casares J., Shahbaz T., et al., 2011, MNRAS, 413, L15  
 Das S., Chattopadhyay I., Nandi A., Molteni D., 2014, MNRAS, 442, 251  
 De Villiers J. P., Hawley J. F., Krolik J. H., Hirose S., 2005, ApJ, 620, 878  
 Debnath D., Chakrabarti S. K., Nandi A., 2008, BASI, 36, 151  
 Debnath D., Chakrabarti S. K., Nandi A., 2013, AdSpR, 52, 2143  
 Dunn R. J. H., Fender R. P., Kording E. G., et al., 2011, MNRAS, 403, 61  
 Dunn R. J. H., Fender R. P., Kording E. G., et al., 2011, MNRAS, 411, 337  
 Ebisawa K., Ogawa M., Aoki T., et al., 1994, PASJ, 46, 375  
 Esin A. A., McClintock J. E., Narayan R., 1997, ApJ, 489, 865  
 Farinelli R., Amati L., Shaposhnikov N., et al., 2013, MNRAS, 428, 3295  
 Fender R. P., Belloni T., Gallo E., 2004, MNRAS, 355, 1105  
 Fender R. P., Homan J., Belloni T., 2009, MNRAS, 396, 1307  
 Feroci R., Matt G., Pooley G., Costa E., et al., 1999, A&A, 351, 985  
 Garnavich P. M., Stanek K. Z., Berlind P., 1999, IAUC, 7276  
 Gierlinski M., Done C., 2004, MNRAS, 347, 885  
 Giri K., Chakrabarti S. K., 2013, MNRAS, 430, 2836  
 Homan J., Belloni T., 2005 Ap&SS, 300, 107  
 Ingram A., Done C., 2011, MNRAS, 415, 2323  
 Lee, S., Ryu, D., Chattopadhyay, I., 2011, ApJ, 728, 142  
 Mandal S., Chakrabarti S. K., 2010, ApJ, 710, L147  
 Markwardt C. B., 2001, Astrophysics & Space science, 276, 209  
 Markwardt C. B., 2009, ASPC, 411, 251  
 McClintock J. E., Remilard R. A., 2006, ‘Black hole binaries’, Compact Stellar X-ray sources, edited by Lewin W. H. G. and M. van der Klis  
 McClintock J. E., Remilard R. A., Rupen M. P., et al., 2009, ApJ, 698, 1398  
 McCollough M. L., Wilson C. A., 1999, IAUC, 7282  
 McKinney J. C., Gammie C. F., 2004, ApJ, 611, 977  
 Meier D. L., Nakamura M., Proceedings 3-D signatures in Stellar explosions, ed. P. Hoefflich, P. Kumar, C. Wheeler, 2004, Cambridge University press, 219  
 Merloni A., Fabian A. C. and Ross R. R., 2000, MNRAS, 313, 193  
 Meyer F., Liu B. F., Meyer-Hofmeister E., 2007, A&A, 463, 1  
 Meyer-Hofmeister E., Liu B. F., Meyer F., 2009, A&A, 508, 329  
 Miller-Jones J. C. A., Sivakoff G. R., Altamirano D., et al., 2012, MNRAS, 421, 468  
 Miyamoto S., Kimura K., Kitamoto S., et al., 1991, ApJ, 383, 784  
 Molteni D., Sponholz H., Chakrabarti S. K., 1996, ApJ, 457, 805  
 Motta S., Belloni T., Homan J., 2009, MNRAS, 400, 1603  
 Motta S., Munoz-Darias T., Casella P., et al., 2011, MNRAS, 418, 2292  
 Munoz-Darias T., Motta S. and Belloni T., 2010, MNRAS, 410, 679  
 Nandi A., Chakrabarti S. K., Vadawale S. V., Rao A. R., 2001, A&A, 380, 245  
 Nandi A., Debnath D., Mandal S., Chakrabarti S. K., 2012, A&A, 542, 56  
 Nandi, A. & Radhika. D, 2012, COSPAR Scientific Assembly,



Mysore, INDIA  
Nandi, A., Radhika. D, Seetha. S., 2013, ASI Conference Series, 8, 71 (arxiv : 1308.4567)  
Nandi A. et al. (in prep.)  
Okuda T., Teresi V., Molteni D., 2007, MNRAS, 377, 1431  
Pooley G. G., Hjellming R. M., 1999, IAUC, 7278  
Radhika. D, Nandi A., S. Seetha, 2013, MmSAI, 84, 624 (arxiv : 1301.7234)  
Radhika. D et al. (in prep.)  
Remilard R. A. et al., 1999, ApJ, 552, 397  
Rodriguez J., Prat L., 2008, Proceedings of Science, 7th INTEGRAL workshop (arxiv : 0811:3519)  
Rodriguez J., Varniere P., 2011, ApJ, 735, 79  
Ryu D., Chakrabarti S. K., Molteni D., 1997, ApJ, 474, 378  
Shakura N. I., Sunyaev R. A., 1973, A&A, 24, 337  
Shaposhnikov N, Titarchuk L., 2007, ApJ, 663, 445  
Shaposhnikov N, Titarchuk L., 2009, ApJ, 699, 453  
Sobczak G. J., McClintock J. E., Remilard R. A., et al., 2000, ApJ, 531, 537  
Soleri P., Belloni T., Casella P., 2008, MNRAS, 383, 10989  
Stiele H., Belloni T. M., Kalemci E., Motta S., 2013, MNRAS, 429, 2655  
Tagger M., Pellat R., 1999, A&A, 349, 1003  
Titarchuk L. G., 1994, ApJ, 434, 570  
Titarchuk, L. G., Fiorito, R. 2004, ApJ, 612, 988  
Titarchuk L., Shaposhnikov N., & Arefiev V., 2007, ApJ, 660, 556  
Titarchuk L., Shaposhnikov N., 2010, ApJ, 724, 1147  
Titarchuk L., Osherovich V., 2000, ApJ, 542, L111  
Vadawale S. V., Rao A. R., Nandi A., Chakrabarti S. K., 2001, A&A, 370, L17  
Wagner R. M., Schmidt G. D., Shrader C. R., 1999, IAUC, 7279  
Wood A., Smith D. A., Marshall F. E., Swank J. H., 1999, IAUC, 7274  
Yang J., Brocksopp C., Corbel S., et al., 2010, MNRAS, 409, L64  
Zhang W., Jahoda K., Swank J. H., et al., 1995, ApJ, 449, 930